Non-periodic finite-element formulation of Kohn-Sham Density Functional Theory

Phanish Suryanarayana [a] Vikram Gavini [b] Thomas Blesgen [c]

Kaushik Bhattacharya [a,*] Michael Ortiz [a]

[a] *Division of Engineering and Applied Science, California Institute of Technology, CA 91125, USA*

[b] *Department of Mechanical Engineering, University of Michigan, MI 48109-2125, USA*

[c] *Max Planck Institute for Mathematics in the Sciences, Inselstraβe 22-26, D-04103 Leipzig, Germany*

Abstract

In this paper, we present a real space, non-periodic, finite-element formulation for Kohn-Sham Density Functional Theory (KS-DFT). In doing so, we transform the original variational problem into a local form by rewriting it as a saddle point problem and show its well posedness by proving the existence of minimizers. Using Γ-convergence, we also prove the convergence of the finite-element approximation along with numerical quadratures. We demonstrate a parallel finite-element implementation of this formulation capable of performing both 'all electron' and pseudopotential calculations through a number of examples for which the results are in very good agreement with those in literature. We also evaluate the numerical performance of this implementation with regard to its scalability and convergence rates. This work lays the foundation for a multiscale approach for studying defects like vacancies, dislocations and cracks that require both quantum mechanical resolution at the core and are also sensitive to long range continuum forces.

Key words: Finite-elements; Kohn-Sham; Density Functional Theory; Γ-convergence

1 Introduction

The Schrödinger equation is fundamental for describing the quantum mechanical electronic structure of matter since it does not need any empirical input. Therefore, in principle we should be able to accurately predict the properties of any system of interest by taking recourse to this equation. Unfortunately, the computations associated with solving this equation are extremely expensive limiting the system size to about ten electrons (Kohn (1999)). Therefore, a number of approaches have been proposed to reduce the computational expense involved, including the vastly popular Density Functional Theory (DFT) which was provided a rigorous mathematical foundation by the work of Hohenberg and Kohn (1964). In it, they demonstrate the existence of a one to one mapping between the ground state electron density and the ground state wavefunction of a many particle system. Therefore, the charge density replaces the many body electronic wavefunction as the basic variable, thereby greatly reducing the complexity of the problem. The most common present day implementation of DFT is through the Kohn-Sham method (Kohn and Sham (1965)) in which the intractable many body problem of interacting electrons in an external potential is reduced to a tractable problem of non-interacting electrons moving in an effective potential. Although in principle this approach is exact, hidden in this formulation is the unknown exchange and correlation functional for which various approximations exist, the most popular ones being the LSDA (Kohn and Sham (1965)) and the Generalized Gradient Approximation (GGA) (Langreth and Mehl (1983); Perdew et al. (1992)).

* Corresponding Author (*bhatta@caltech.edu)*

The plane wave basis is one of the most frequently used basis for solving the Kohn-Sham problem (Kresse and Furthmüller (1996); Segall et al. (2002); Gonze et al. (2002); Ismail-Beigi and Arias (2000)) because of a number of attractive features. Namely, it forms a complete and orthonormal set which is independent of the atomic positions, forces corresponding to the basis set corrections do not exist, efficient calculations of convolutions are possible using Fast Fourier Transform (FFT) and there is monotonic decrease in the energy with increasing basis set. On the other hand, the plane wave basis also suffers from a few notable disadvantages. Firstly, the plane wave basis is ideal for problems with periodic boundary conditions. Therefore, the study of non-periodic and localized systems such as defects, clusters and surfaces requires the introduction of artificial periodicity by means of a supercell approach which can lead to spurious results. Secondly, the plane wave basis functions are non-local in real space, resulting in dense matrices which are not amenable to iterative solution methods, therefore limiting their usefulness in multiscale approaches which are usually formulated in real space to accommodate non-periodic boundary conditions. Consequently, there have been efforts over the past decade directed towards performing DFT calculations in real space (Pask et al. (1999); Hehre et al. (1969); Wills and Cooper (1987); Soler et al. (2002); Skylaris et al. (2005); Bowler et al. (2006); Chelikowsky et al. (1994); Castro et al. (2006)).

In this paper, we present a non-periodic, real space, finite-element formulation and implementation of KS-DFT with LSDA as the exchange and correlation functional. This work bears similarity to the one carried out by Gavini et al. (2007b) who worked on the simpler orbital-free version of DFT. The present formulation is not restricted by the choice of exchange correlation functional and other commonly used functionals like the GGA can be easily incorporated. We intend to use the framework developed in this paper as a stepping stone towards our final goal of studying defects in solids like vacancies, dislocations and cracks. To achieve this, the present work needs to be embedded into a coarse grained,

seamless, atomistic-continuum formulation of KS-DFT. This is a subject of ongoing research following Gavini et al. (2007a).

The approaches adopted for solving the Kohn-Sham problem can be broadly classified as ones which use the Self-Consistent Field (SCF) method and others in which some form of constrained direct minimization is performed (Payne et al. (1992)). The equivalence of the variational and eigenvalue problems is shown in Section 3.1, thereby showing the above mentioned approaches to be equivalent. One of the most time consuming part of any real space implementation is the evaluation of the non-local electrostatic interactions. To overcome this, we rewrite the electrostatic contributions to the energy as a local variational principle, thereby reformulating the original minimization problem as a saddle point problem and subsequently discretize it using finite-elements. In Section 3.2 we show that this saddle point problem is mathematically well-posed by proving existence of solutions. Further, we prove the convergence of the finite-element approximation, including numerical quadratures using Γ-convergence in Sections 3.3 and 3.4. A similar analysis is presented for a model with the pseudopotential approximation in Section 3.5. In the pseudopotential approximation, the core electrons are excluded from the calculations and their effect on the system is mimicked by an effective external potential which additionally enforces the valence pseudo-wavefunctions to be nodeless, thereby substantially reducing the computational effort. Therefore, the pseudopotential approximation is an attractive one and is universally used, almost always.

Subsequently, we turn to the parallel numerical implementation of KS-DFT using finite-elements in Section 4. The main features of the method include coarsening of the mesh away from the nuclei and convecting this mesh with the nuclei position so as to obtain rapid convergence on displacing the nuclei. Using the advantageous features of both the SCF method and Newton's method, we propose a hybrid numerical scheme wherein a sequence of triangulations using a subdivision algorithm are generated, the coarsest of

which is used to solve the eigenvalue problem using the SCF approach and the rest are used to solve the constrained optimization problem using Newton's method. The solution obtained on a particular triangulation is interpolated and used as starting guess for the next triangulation generated, resulting in quadratic convergence. The procedure is carried out until the solution converges with respect to mesh size. The forces required to find the equilibrium position of the nuclei are derived in Section 5.

In Section 6, we verify the numerical implementation by testing it on a number of examples which range from single atoms to small clusters. To test the accuracy of the method, 'all electron' calculations which include the core electrons have been performed for a few atoms and molecules. Since 'all electron' calculations become prohibitively expensive as the system size increases, we incorporate the 'Evanescent Core' (Fiolhais et al. (1995)) and Troullier Martins (Troullier and Martins (1991)) pseudopotentials. We also look at the performance of the implementation by investigating its scaling with increasing number of nodes, its parallel scaling and the finite-element convergence rates obtained. Finally, we conclude in Section 7.

2 Formulation

The theoretical framework of DFT has its origins in the Hohenberg-Kohn theorems (Hohenberg and Kohn (1964)). The first theorem is related to uniqueness and states that the ground state expectation value of any observable is a unique functional of the exact ground state electron density. The second theorem sheds light on the variational structure of the problem and shows that the electron density that minimizes the total energy is the exact ground state density. The problem of finding the ground state energy and electron density is equivalent to the problem of minimizing the energy of a system of non-interacting electrons in a mean-field. The corresponding energy functional

$\mathcal{E} : X \times \mathbb{R}^{SM} \to \mathbb{R}$ where X is a suitable space of solutions for the orthogonal wavefunctions is given by (Parr and Yang (1989); Finnis (2003))

$$\mathcal{E}(\Psi, \mathbf{R}) = T_{\rm s}(\rho_\alpha, \rho_\beta) + E_{\rm xc}(\rho_\alpha, \rho_\beta) + E_{\rm H}(\rho_\alpha + \rho_\beta) + E_{\rm ext}(\rho_\alpha + \rho_\beta, \mathbf{R}) + E_{\rm zz}(\mathbf{R}) \,, \quad (1)$$

where

$$\rho_\alpha(\mathbf{x}) = \sum_{i=1}^{N_\alpha} \psi_{i\alpha}^*(\mathbf{x})\psi_{i\alpha}(\mathbf{x}) = \sum_{i=1}^{N_\alpha} |\psi_{i\alpha}(\mathbf{x})|^2 \,, \quad (2)$$

$$\rho_\beta(\mathbf{x}) = \sum_{i=1}^{N_\beta} \psi_{i\beta}^*(\mathbf{x})\psi_{i\beta}(\mathbf{x}) = \sum_{i=1}^{N_\beta} |\psi_{i\beta}(\mathbf{x})|^2 \quad (3)$$

represent the electron densities with the spin component 'up' and 'down' respectively and $\rho(\mathbf{x}) = \rho_\alpha(\mathbf{x}) + \rho_\beta(\mathbf{x})$ is the total electron density. By $\Psi = \{\psi_{1\alpha}, \psi_{2\alpha}, \ldots, \psi_{N_\alpha\alpha}, \psi_{1\beta}, \psi_{2\beta}, \ldots, \psi_{N_\beta\beta}\}$, we denote the vector of wavefunctions and $\mathbf{R} \in \mathbb{R}^{SM}$ is a collection of all the nuclear positions $\mathbf{R} = \{\mathbf{R}_1, \mathbf{R}_2, \ldots, \mathbf{R}_M\}$, $S \geq 1$ denotes the space dimension and $M \in \mathbb{N}$ is the number of nuclei. The wavefunctions are orthonormal, thereby satisfying the relation

$$\int \psi_{i\sigma}^*(\mathbf{x})\psi_{j\sigma}(\mathbf{x}) \, \mathrm{d}\mathbf{x} = \delta_{ij} \,, \qquad \sigma \in \{\alpha, \beta\}. \quad (4)$$

N_α and N_β represent the number of electrons with spin 'up' and 'down' respectively,

$$N_\alpha = \int \rho_\alpha(\mathbf{x}) \, \mathrm{d}\mathbf{x} \,, \qquad N_\beta = \int \rho_\beta(\mathbf{x}) \, \mathrm{d}\mathbf{x}. \quad (5)$$

Note that if the domain of integration is not specified, it refers to all of space $\mathbb{R}^S$. Let us look at each of the terms in Eqn. (1). The first term $T_s(\rho_\alpha, \rho_\beta)$ represents the kinetic energy of the non-interacting electrons. $E_{\rm xc}(\rho_\alpha, \rho_\beta)$ denotes the exchange and correlation energy for which we use the LSDA in which the exchange correlation energy is taken to be that of a uniform electron gas having the same density (Kohn and Sham (1965)). $E_{\rm H}$, $E_{\rm ext}$ and $E_{\rm zz}$ are electrostatic terms with $E_{\rm H}$ known as the Hartree energy representing the classical electrostatic interaction energy of the electron density, $E_{\rm ext}$ is the interaction energy with the external potential $V_{\rm ext}$ induced by the nuclear charges and $E_{\rm zz}$ denotes

the repulsive energy between the nuclei. The expressions for each of these terms is given below:

$$T_{\rm s}(\rho_\alpha,\rho_\beta) = -\frac{1}{2}\sum_{\sigma}\sum_{i=1}^{N_\sigma}\int \psi_{i\sigma}^{*}(\mathbf{x})\nabla^2\psi_{i\sigma}(\mathbf{x})\,{\rm d}\mathbf{x}\,, \tag{6}$$

$$E_{\rm H}(\rho) = \frac{1}{2}\int\int \frac{\rho(\mathbf{x})\rho(\mathbf{x}')}{|\mathbf{x}-\mathbf{x}'|}\,{\rm d}\mathbf{x}\,{\rm d}\mathbf{x}'\,, \tag{7}$$

$$E_{\rm ext}(\rho,\mathbf{R}) = \int \rho(\mathbf{x})V_{\rm ext}(\mathbf{x},\mathbf{R})\,{\rm d}\mathbf{x}\,, \tag{8}$$

$$E_{\rm zz}(\mathbf{R}) = \frac{1}{2}\sum_{I=1}^{M}\sum_{\substack{J=1\\J\neq I}}^{M}\frac{Z_I Z_J}{|\mathbf{R}_I-\mathbf{R}_J|}. \tag{9}$$

The exchange and correlation energy can be separated into individual contributions from the exchange and correlation parts,

$$E_{\rm xc}(\rho_\alpha,\rho_\beta) = E_{\rm x}(\rho_\alpha,\rho_\beta) + E_{\rm c}(\rho_\alpha,\rho_\beta). \tag{10}$$

The expression for the exact exchange energy $E_{\rm x}(\rho_\alpha,\rho_\beta)$ of an uniform electron gas is

$$E_{\rm x}(\rho_\alpha,\rho_\beta) = -\frac{3}{4}\left(\frac{6}{\pi}\right)^{1/3}\int(\rho_\alpha^{4/3}(\mathbf{x})+\rho_\beta^{4/3}(\mathbf{x}))\,{\rm d}\mathbf{x}\,, \tag{11}$$

and the correlation energy $E_{\rm c}(\rho_\alpha,\rho_\beta)$ can be written as

$$E_{\rm c}(\rho_\alpha,\rho_\beta) = \int \varepsilon_{\rm c}(\rho_\alpha(\mathbf{x}),\rho_\beta(\mathbf{x}))\rho(\mathbf{x})\,{\rm d}\mathbf{x}. \tag{12}$$

For the correlation term, we use the parametrization provided by Perdew and Wang (1992) which has been fitted to very accurate Monte Carlo simulations carried out by Ceperley and Alder (1980):

$$\varepsilon_c(\rho_\alpha,\rho_\beta) = \varepsilon_c(r_s,0) + \alpha_c(r_s)\frac{f(\zeta)}{f''(0)}(1-\zeta^4) + [\varepsilon_c(r_s,1)-\varepsilon_c(r_s,0)]f(\zeta)\zeta^4\,, \tag{13}$$

where

$$r_s = \left[\frac{3}{4\pi(\rho_\alpha + \rho_\beta)}\right]^{1/3}, \tag{14}$$

$$\zeta = \frac{\rho_\alpha - \rho_\beta}{\rho_\alpha + \rho_\beta}, \tag{15}$$

$$f(\zeta) = \frac{[(1+\zeta)^{4/3} + (1-\zeta)^{4/3} - 2]}{2^{4/3} - 2}. \tag{16}$$

$\varepsilon_c(r_s, 0)$, $\varepsilon_c(r_s, 1)$ and $-\alpha_c(r_s)$ have been fitted to the following analytic expression whose parameters can be found in Perdew and Wang (1992)

$$G(r_s, A, \alpha_1, \beta_1, \beta_2, \beta_3, \beta_4, p) = \\ -2A(1+\alpha_1 r_s)\ln\left(1 + \frac{1}{2A(\beta_1 r_s^{1/2} + \beta_2 r_s + \beta_3 r_s^{3/2} + \beta_4 r_s^{p+1})}\right). \tag{17}$$

The electrostatic interaction energy and the repulsive energy of the nuclei are non-local in nature, and thus are not amenable to a local discretization. Therefore, we rewrite them into a local form for which we adopt the following strategy. We represent the nuclear charge of magnitude Z_I at a site R_I by a regularized bounded charge distribution with a compact support in a neighborhood of a small ball around R_I given by $-Z_I\delta_{R_I}(\mathbf{x})$ (it is convention in electronic structure calculations to associate a negative charge with nuclei and a positive charge with electrons), such that $\int_{\mathbb{R}^3} \delta_{R_I}(\mathbf{x})\,\mathrm{d}\mathbf{x} = 1$ for $1 \leq I \leq M$. We note that the electrostatic potential due to these regularized charge distributions is pointwise bounded. Defining $b(\mathbf{x}, \mathbf{R})$ as the sum of all such regularized charge distributions of the M nuclei present in the system,

$$b(\mathbf{x}, \mathbf{R}) = -\sum_{I=1}^{M} Z_I \delta_{R_I}(\mathbf{x}), \tag{18}$$

the nuclear repulsive energy can be rewritten as

$$E_{\text{zz}}(\mathbf{R}) = \frac{1}{2}\int\int \frac{b(\mathbf{x}, \mathbf{R})b(\mathbf{x}', \mathbf{R})}{|\mathbf{x} - \mathbf{x}'|}\,\mathrm{d}\mathbf{x}\,\mathrm{d}\mathbf{x}'. \tag{19}$$

Therefore the electrostatic potential due to the nuclei and electron charge distribution can

be computed as a solution to the Poisson equation

$$\frac{-1}{4\pi}\nabla^2\phi(\mathbf{x},\mathbf{R}) = \rho(\mathbf{x}) + b(\mathbf{x},\mathbf{R}). \tag{20}$$

The above equation has an unique solution given by

$$\phi(\mathbf{x},\mathbf{R}) = \int \frac{\rho(\mathbf{x}')}{|\mathbf{x}-\mathbf{x}'|}\,\mathrm{d}\mathbf{x}' + \int \frac{b(\mathbf{x}',\mathbf{R})}{|\mathbf{x}-\mathbf{x}'|}\,\mathrm{d}\mathbf{x}' = V_{\mathrm{H}}(\mathbf{x}) + V_{\mathrm{ext}}(\mathbf{x},\mathbf{R}). \tag{21}$$

Hence we can write the following variational problem for which the associated Euler-Lagrange equation is given by Eqn. (20):

$$\begin{aligned}&\frac{1}{2}\int\int \frac{\rho(\mathbf{x})\rho(\mathbf{x}')}{|\mathbf{x}-\mathbf{x}'|}\,\mathrm{d}\mathbf{x}\,\mathrm{d}\mathbf{x}' + \int \rho(\mathbf{x})V_{\mathrm{ext}}(\mathbf{x})\,\mathrm{d}\mathbf{x} + \frac{1}{2}\int\int \frac{b(\mathbf{x})b(\mathbf{x}')}{|\mathbf{x}-\mathbf{x}'|}\,\mathrm{d}\mathbf{x}\,\mathrm{d}\mathbf{x}' \\ &= -\inf_{\phi\in H_0^1(\mathbb{R}^S)}\left\{\frac{1}{8\pi}\int |\nabla\phi(\mathbf{x},\mathbf{R})|^2\mathrm{d}\mathbf{x} - \int(\rho(\mathbf{x}) + b(\mathbf{x},\mathbf{R}))\phi(\mathbf{x},\mathbf{R})\,\mathrm{d}\mathbf{x}\right\}.\end{aligned} \tag{22}$$

Further Eqn. (22) has a unique solution, and this solution satisfies Eqn. (20). Using the above relation we can write Eqn. (1) as the variational problem

$$\mathcal{E}(\Psi,\mathbf{R}) = \sup_{\phi\in H_0^1(\mathbb{R}^S)} \mathcal{L}(\Psi,\mathbf{R},\phi)\,, \tag{23}$$

where

$$\begin{aligned}\mathcal{L}(\Psi,\mathbf{R},\phi) = &-\frac{1}{2}\sum_{\sigma}\sum_{i=1}^{N_\sigma}\int \psi_{i\sigma}^*(\mathbf{x})\nabla^2\psi_{i\sigma}(\mathbf{x})\,\mathrm{d}\mathbf{x} + E_{\mathrm{xc}}(\rho_\alpha,\rho_\beta) - \frac{1}{8\pi}\int|\nabla\phi(\mathbf{x},\mathbf{R})|^2\mathrm{d}\mathbf{x} \\ &+ \int(\rho(\mathbf{x}) + b(\mathbf{x},\mathbf{R}))\phi(\mathbf{x},\mathbf{R})\,\mathrm{d}\mathbf{x}.\end{aligned} \tag{24}$$

The problem of determining the ground state electron density and the equilibrium positions of the nuclei can now be expressed as the saddle point problem,

$$\inf_{\substack{\Psi\in(H_0^1(\mathbb{R}^S))^N\\ \mathbf{R}\in\mathbb{R}^{SM}}} \mathcal{E}(\Psi,\mathbf{R}) = \inf_{\substack{\Psi\in(H_0^1(\mathbb{R}^S))^N\\ \mathbf{R}\in\mathbb{R}^{SM}}} \sup_{\phi\in H_0^1(\mathbb{R}^S)} \mathcal{L}(\Psi,\mathbf{R},\phi) \tag{25}$$

subject to the following constraints

$$\int \psi_{i\sigma}^*(\mathbf{x})\psi_{j\sigma}(\mathbf{x})\,d\mathbf{x} = \delta_{ij}\,, \qquad \sigma\in\{\alpha,\beta\}, \quad i,j\in\{1,2,\ldots,N_{\alpha,\beta}\}. \tag{26}$$

N_α, N_β need to be chosen such that the system has the lowest possible energy amongst all possible combinations of N_α, N_β subject to the constraint of the total number of the electrons in the system being studied, i.e. $N_\alpha + N_\beta = N$.

3 Properties of the Kohn-Sham variational problem

In the present section, for the sake of clarity we will neglect spin polarization, thereby reducing the LSDA to the Local Density Approximation (LDA). This simplification is not essential, and the results hold for LSDA. Corresponding to Eqn. (1), for LDA we have

$$\mathcal{E}(\Psi,\mathbf{R}) = -\frac{1}{2}\sum_{i=1}^{N}\int \psi_i^*(\mathbf{x})\nabla^2\psi_i(x)\,\mathrm{d}\mathbf{x} + E_{\mathrm{xc}}(\rho) + E_{\mathrm{H}}(\rho) + E_{\mathrm{ext}}(\rho,\mathbf{R}) + E_{\mathrm{zz}}(\mathbf{R})\,, \quad (27)$$

where $E_{\mathrm{xc}}(\rho)$ can be obtained from the earlier definition by setting $\zeta = 0$, and all the other terms remain the same; $\rho(\mathbf{x}) = \sum_{i=1}^{N}|\psi_i(\mathbf{x})|^2$ and $\Psi = \{\psi_1, \psi_2, \ldots, \psi_N\}$. Also, to avoid technical problems, we restrict our analysis to a bounded subset Ω of $\mathbb{R}^S$. With this simplification we obtain the variational problem

$$\inf_{\substack{\Psi\in(H_0^1(\Omega))^N \\ \mathbf{R}\in\mathbb{R}^{SM}}} \mathcal{E}(\Psi,\mathbf{R}) = \inf_{\substack{\Psi\in(H_0^1(\Omega))^N \\ \mathbf{R}\in\mathbb{R}^{SM}}} \sup_{\phi\in H_0^1(\Omega)} \mathcal{L}(\Psi,\mathbf{R},\phi) \quad (28)$$

subject to the constraints $\int_\Omega \psi_i^*(\mathbf{x})\psi_j(\mathbf{x})\mathrm{d}\mathbf{x} = \delta_{ij}$.

3.1 Equivalence of variational and eigenvalue problems

We show the equivalence of the variational and eigenvalue problems in this section. The proof is similar in spirit to Roothaan (1951) where it has been demonstrated for the Hartree Fock equations, and is provided here for the sake of completeness. Using La-

grange multipliers to enforce the constraints, we obtain the following functional

$$\mathcal{E}_c(\Psi,\mathbf{R},\Lambda)=\mathcal{E}(\Psi,\mathbf{R})-\sum_{i=1}^{N}\sum_{j=1}^{N}\lambda_{ij}\left(\int_\Omega \psi_i^*(\mathbf{x})\psi_j(\mathbf{x})\,\mathrm{d}\mathbf{x}-\delta_{ij}\right), \tag{29}$$

where λ_{ij} are the Lagrange multipliers. Let us first prove that the matrix $\Lambda=(\Lambda_{ij})_{1\le i,j\le N}$ is Hermitian. Taking variations of Eqn. (29), and setting it to zero we obtain

$$\left(-\frac{1}{2}\nabla^2+V_{\text{eff}}(\mathbf{x},\mathbf{R})\right)\psi_i(\mathbf{x})=\sum_{j=1}^{N}\lambda_{ij}\psi_j(\mathbf{x}), \tag{30}$$

$$\left(-\frac{1}{2}\nabla^2+V_{\text{eff}}(\mathbf{x},\mathbf{R})\right)\psi_i^*(\mathbf{x})=\sum_{j=1}^{N}\lambda_{ji}\psi_j^*(\mathbf{x}), \tag{31}$$

$$\int_\Omega \psi_i^*(\mathbf{x})\psi_j(\mathbf{x})\,\mathrm{d}\mathbf{x}=\delta_{ij}, \tag{32}$$

where

$$V_{\text{eff}}(\mathbf{x},\mathbf{R})=V_{\text{ext}}(\mathbf{x},\mathbf{R})+V_{\text{H}}(\mathbf{x})+\frac{\delta E_{\text{xc}}(\rho)}{\delta\rho(\mathbf{x})}. \tag{33}$$

Taking the complex conjugate of Eqn. (31) and subsequently subtracting it from Eqn. (30) we obtain the following relation

$$\sum_{j=1}^{N}(\lambda_{ij}-\lambda_{ji}^*)\psi_j(\mathbf{x})=0. \tag{34}$$

Since the ψ_j are linearly independent it follows that $\lambda_{ij}=\lambda_{ji}^*$, showing the matrix Λ to be indeed Hermitian. Hence, we obtain the following system of equations which can be written in matrix form as

$$\mathcal{H}\Psi=\Psi\Lambda, \qquad \mathcal{H}=-\frac{1}{2}\nabla^2+V_{\text{eff}}(\mathbf{x},\mathbf{R}). \tag{35}$$

Now let us subject the wavefunctions to a unitary transformation, and the matrix Λ to a similarity transformation

$$\hat{\Psi}=\Psi Q, \qquad \hat{\Lambda}=Q^*\Lambda Q \tag{36}$$

with $QQ^* = Q^*Q = \mathbf{I}$, $\mathbf{I}$ being the identity matrix. Since unitary transformations are norm conserving, the electron density is left invariant:

$$\rho(\mathbf{x}) = \sum_{i=1}^{N} |\psi_i(\mathbf{x})|^2 = \sum_{i=1}^{N} |\hat{\psi}_i(\mathbf{x})|^2. \tag{37}$$

Using the above relations we get

$$\hat{\mathcal{H}}\hat{\Psi} = \hat{\Psi}\hat{\Lambda} \tag{38}$$

where $\mathcal{H} = \hat{\mathcal{H}}$. Hence the wavefunctions on unitary transformation satisfy equations of exactly the same form as the original ones prior to transformation. Since the matrix Λ is Hermitian, there exists an unitary matrix Q such that $\hat{\Lambda}$ is a real diagonal matrix. Therefore, without any loss of generality we can replace Eqn. (35) with the eigenvalue problem

$$\mathcal{H}\psi_i = \epsilon_i \psi_i \quad 1 \leq i \leq N. \tag{39}$$

The above equations are said to be in *canonical form*.

3.2 Existence of a Minimum

In this section, we establish the existence of a minimum for the Kohn-Sham variational principle. The main result is Theorem 1. We introduce a suitable space of solutions X corresponding to normalized orthogonal wavefunctions as

$$X = \left\{ \tilde{\Psi} \in (H_0^1(\Omega))^N \;\middle|\; \langle \tilde{\psi}_i, \tilde{\psi}_j \rangle_{(L^2(\Omega),L^2(\Omega))} = \delta_{ij}, \;\; i,j = 1,2,\ldots,N \right\}. \tag{40}$$

We require that Ω is an open, bounded subset of $\mathbb{R}^S$ with Lipschitz boundary. We point out that if we additionally postulate that Ω is a dyadic cube, then all the subsequent results of this analysis also hold for

$$X = \left\{ \tilde{\Psi} \in (H^1_{\text{per}}(\Omega))^N \;\middle|\; \langle \tilde{\psi}_i, \tilde{\psi}_j \rangle_{(L^2(\Omega),L^2(\Omega))} = \delta_{ij}, \;\; i,j = 1,2,\ldots,N \right\}, \tag{41}$$

which corresponds to a periodic system. By $H^1_{\text{per}}(\Omega)$ we denote the space of Sobolev functions on the torus obtained by identifying the opposite sides of Ω.

On integrating by parts, the energy of the system as expressed by Eqn. (1) can be rewritten in a generic form as

$$\mathcal{E}(\Psi,\mathbf{R}) = \sum_{i=1}^{N} \frac{1}{2}\int_{\Omega} |\nabla\psi_i(\mathbf{x})|^2 \mathrm{d}\mathbf{x} + J(\rho,\mathbf{R}) + G(\rho), \qquad \rho(\mathbf{x}) = \sum_{i=1}^{N} |\psi_i(\mathbf{x})|^2, \tag{42a}$$

$$J(\rho,\mathbf{R}) = -\min_{\phi\in H^1_0(\Omega)} \left\{ \frac{1}{8\pi}\int_{\Omega} |\nabla\phi(\mathbf{x},\mathbf{R})|^2 \mathrm{d}\mathbf{x} - \int_{\Omega} (\rho(\mathbf{x}) + b(\mathbf{x},\mathbf{R}))\phi(\mathbf{x},\mathbf{R})\,\mathrm{d}\mathbf{x} \right\} + \Sigma, \tag{42b}$$

$$G(\rho) = \int_{\Omega} g(\rho)\,\mathrm{d}\mathbf{x}. \tag{42c}$$

The term Σ specifies the self energy of the nuclear charges which is an inconsequential constant in this analysis and hence will be dropped later.

We make the following hypothesis on g:

(A1) The density g is continuous in $\overline{\Omega}$.

(A2) The growth condition $|g(t)| \leq c_2|t|^q + c_1$ holds for positive real constants c_2, c_1 and the exponent satisfies

$$q \in \begin{cases} \left[1, \frac{S}{S-2}\right), & \text{if } S > 2, \\ [1, +\infty), & \text{otherwise.} \end{cases}$$

(A3) The exponent q fulfills $2q < 3$.

The Assumption (A3) will become clear in the proof of Lemma 3.

Let the dual exponent p^* of p be given by $1/p^* = 1/p - 1/S$. We first note the following

results:

(a) For $\rho \in L^2(\Omega)$ the functional $J(\rho, \mathbf{R})$ is well defined, i.e. its corresponding minimization problem admits a minimum. This result follows from the Poincaré inequality and the Lax-Milgram Lemma. It is also easy to check that $\rho \in L^2(\Omega)$ if $2^* > 4$.

(b) The functional J is continuous in $L^2(\Omega)$.

(c) The functional G is continuous in $L^q(\Omega)$, which follows from the continuity of g and the growth condition (A2).

(d) As $\sum_{i=1}^{N} \frac{1}{2} \int_\Omega |\nabla \psi_i(\mathbf{x})|^2 \mathrm{d}\mathbf{x}$ is continuous in the strong topology of $(H_0^1(\Omega))^N$ and convex, it follows that $\psi \mapsto \sum_{i=1}^{N} \frac{1}{2} \int_\Omega |\nabla \psi_i(\mathbf{x})|^2 \mathrm{d}\mathbf{x}$ is lower semi-continuous in the weak topology of $(H_0^1(\Omega))^N$.

Lemma 1 *X is closed in the weak topology of $(H_0^1(\Omega))^N$.*

Proof. Consider an arbitrary sequence $(\Psi_l)_l \subset X$ with $\Psi_l \rightharpoonup \Psi$ in $(H_0^1(\Omega))^N$. By the Rellich-Kondrakov theorem (Rudin (1991)), $H_0^1(\Omega)$ has a compact embedding into $L^2(\Omega)$. Thus $(\psi_{i,l})_l \to \psi_i$ in $L^2(\Omega)$ for $i = 1, 2, \ldots, N$ from which it follows that $\delta_{ij} = \langle \psi_{i_l} | \psi_{j_l} \rangle_{(L^2(\Omega), L^2(\Omega))} \to \langle \psi_i | \psi_j \rangle_{(L^2(\Omega), L^2(\Omega))}$ for $i, j = 1, 2, \ldots, N$ as $l \to \infty$. Therefore $\Psi \in X$, which implies that X is closed in the weak topology of $(H_0^1(\Omega))^N$. $\square$

Lemma 2 *Let (A1), (A2) hold and $S < 4$. Then $\mathcal{E}$ is lower semi-continuous in the weak topology of X.*

Proof. Consider any sequence $(\Psi_l)_l \subset (H_0^1(\Omega))^N$ such that $\Psi_l \rightharpoonup \Psi$ in $(H_0^1(\Omega))^N$. As $H_0^1(\Omega)$ has a compact embedding into $L^4(\Omega)$ for $S < 4$, it follows that $(\psi_{i,l})_l \to \psi_i$ in $L^4(\Omega)$ for $i = 1, 2, \ldots, N$. Hence $(\psi_{i,l}^2)_l \to \psi_i^2$ in $L^2(\Omega)$ and therefore $(\rho_l)_l \to \rho$ in $L^2(\Omega)$. From (A2) it follows that the embedding $H_0^1(\Omega) \hookrightarrow L^{2q}(\Omega)$ is compact. Thus $\rho_l \to \rho$ in $L^{\max\{2,q\}}(\Omega)$. From (b)-(d) it follows that $\sum_{i=1}^{N} \frac{1}{2} \int_\Omega |\nabla \psi_i(\mathbf{x})|^2 \mathrm{d}\mathbf{x}$, $J(\rho, \mathbf{R})$, and

$G(\rho)$ are lower semi-continuous in the weak topology of $(H_0^1(\Omega))^N$. Hence, it follows that $\mathcal{E}$ is lower semi-continuous in the weak topology of $(H_0^1(\Omega))^N$, and as $X \subset (H_0^1(\Omega))^N$, we conclude that $\mathcal{E}$ is lower semi-continuous in the weak topology of X. $\square$

Lemma 3 *Let (A2), (A3) hold. Then $\mathcal{E}$ is coercive in the weak topology of X.*

Proof. We first note the following results on the properties of $J(\rho, \mathbf{R})$:

(i) From the linearity of the Euler-Lagrange equations associated with $J(\rho, \mathbf{R})$, the electrostatic energy of the system can be rewritten as

$$J(\rho, \mathbf{R}) = E_H(\rho) + \int_\Omega V_{\text{ext}}(\mathbf{x}, \mathbf{R})\rho(\mathbf{x})\mathrm{d}\mathbf{x} + L(\mathbf{R}), \tag{43a}$$

$$E_H(\rho) = -\min_{\phi \in H_0^1(\Omega)} \left\{ \frac{1}{8\pi}\int_\Omega |\nabla\phi(\mathbf{x})|^2 \mathrm{d}\mathbf{x} - \int_\Omega \rho(\mathbf{x})\phi(\mathbf{x})\,\mathrm{d}\mathbf{x} \right\}, \tag{43b}$$

where $L(\mathbf{R}) = E_{zz}(\mathbf{R}) + \Sigma$.

We point out that V_{ext} is pointwise bounded. More precisely, it holds $|V_{\text{ext}}(\cdot, \mathbf{R})| \leq C$ almost everywhere in Ω for all $\mathbf{R} \in \mathbb{R}^{SM}$ and some constant C.

(ii) The functional E_H is super-linear, that is $E_H(\rho_1 + \rho_2) \geq E_H(\rho_1) + E_H(\rho_2)$ for arbitrary, point-wise positive ρ_1, $\rho_2 \in L^2(\Omega)$. This follows from the linearity of the corresponding Euler-Lagrange equations.

From (ii) we can directly derive a lower bound for $E_H(\rho)$,

$$\begin{aligned} E_H(\rho) &= E_H\Big(\sum_{i=1}^N |\psi_i|^2\Big) \geq \sum_{i=1}^N E_H(|\psi_i|^2) \\ &\geq \sum_{i=1}^N \left[\max_{\phi_i \in H_0^1(\Omega)} \left\{ \int_\Omega |\psi_i(\mathbf{x})|^2 \phi_i(\mathbf{x})\mathrm{d}\mathbf{x} - \frac{1}{8\pi}\int_\Omega |\nabla\phi_i(\mathbf{x})|^2 \mathrm{d}\mathbf{x} \right\} \right]. \end{aligned} \tag{44}$$

We use $\phi_i = C_0|\psi_i|$ as test functions in Eqn. (44) for a constant C_0 that will be determined later. Additionally, we also recall the following simple result on the weak derivative of an absolute function, whose proof is elementary but can for instance be found in

Gilbarg and Trudinger (1983). If $v \in H^1(\Omega)$, then $|v| \in H^1(\Omega)$ and $\|\nabla|\psi_i|\|_{L^2(\Omega)} \leq \|\nabla\psi_i\|_{L^2(\Omega)}$. Plugging in $\phi_i(\mathbf{x}) = C_0|\psi_i(\mathbf{x})|$ in Eqn. (44) as trial functions for $i = 1, 2, \ldots, N$, we arrive at the following lower bound for $E_H(\rho)$,

$$\begin{aligned} E_H(\rho) &\geq \sum_{i=1}^{N} \left[\max_{\phi_i \in H_0^1(\Omega)} \left\{ \int_\Omega |\psi_i(\mathbf{x})|^2 \phi_i(\mathbf{x}) \mathrm{d}\mathbf{x} - \frac{1}{8\pi} \int_\Omega |\nabla\phi_i(\mathbf{x})|^2 \mathrm{d}\mathbf{x} \right\} \right] \\ &\geq \sum_{i=1}^{N} \left[C_0 \int_\Omega |\psi_i(\mathbf{x})|^3 \mathrm{d}\mathbf{x} - \frac{C_0}{8\pi} \int_\Omega |\nabla\psi_i(\mathbf{x})|^2 \mathrm{d}\mathbf{x} \right] \qquad (45) \\ &= C_0 \|\Psi\|_{L^3(\Omega)}^3 - \frac{C_0}{8\pi} \|\nabla\Psi\|_{L^2(\Omega)}^2. \qquad (46) \end{aligned}$$

Using Eqn. (46) in Eqn. (43a) and $\|V_{\text{ext}}\|_{L^\infty(\Omega)} \leq C$ we conclude

$$J(\rho) \geq C_0 \|\Psi\|_{L^3(\Omega)}^3 - \frac{C_0}{8\pi} \|\nabla\Psi\|_{L^2(\Omega)}^2 - C\|\Psi\|_{L^2(\Omega)}^2. \qquad (47)$$

Finally we require the inequality

$$G(\rho) \geq -c_0 \|\Psi\|_{L^{2q}(\Omega)}^{2q} - c_1. \qquad (48)$$

This is a consequence of the growth condition (A2) on g which yields

$$G(\rho) \geq -c_2 \left\| \sum_{i=1}^{N} |\psi_i|^2 \right\|_{L^q(\Omega)}^q - c_1$$

and observing that by the triangle inequality and positivity of the norm

$$\left\| \sum_{i=1}^{N} |\psi_i|^2 \right\|_{L^q(\Omega)}^q \leq \left[\sum_{i=1}^{N} \|\psi_i\|_{L^{2q}(\Omega)}^2 \right]^q \leq \left[\sum_{i=1}^{N} \|\psi_i\|_{L^{2q}(\Omega)} \right]^{2q} \leq c_3 \|\Psi\|_{L^{2q}(\Omega)}^{2q}.$$

With the help of Eqn. (47) and Eqn. (48) we end up with

$$\mathcal{E}(\Psi, \mathbf{R}) \geq \frac{1}{2} \left(1 - \frac{C_0}{4\pi} \right) \|\nabla\Psi\|_{L^2(\Omega)}^2 + C_0 \|\Psi\|_{L^3(\Omega)}^3 - c_0 \|\Psi\|_{L^{2q}(\Omega)}^{2q} - C\|\Psi\|_{L^2(\Omega)}^2 - c_1. \qquad (49)$$

Choosing $0 < C_0 < 4\pi$, we find that $\|\Psi\|_{L^3(\Omega)}^3$ grows faster than $\|\Psi\|_{L^{2q}(\Omega)}^{2q}$ as $2q < 3$ by (A3), and $\|\Psi\|_{L^2(\Omega)}^2$. This ensures $\mathcal{E}(\Psi) \to +\infty$ as $\|\Psi\|_{(H_0^1(\Omega))^N} \to +\infty$. This is the

coercivity of $\mathcal{E}$ in the weak topology of $(H_0^1(\Omega))^N$. From Lemma 1, as X is closed in the weak topology of $(H_0^1(\Omega))^N$, it follows that $\mathcal{E}$ is coercive in the weak topology of X. □

Theorem 4 *Let (A1)-(A3) hold and let $S < 4$. Then $\mathcal{E}$ has a minimum in X.*

Proof. This is an immediate consequence of Lemma 2 and 3 and the fundamental theorem of the calculus of variations, see e.g. Dal Maso (1993); Struwe (1990). □

The exchange and correlation functionals under LDA approximation satisfy the growth condition (A2) with $q = 4/3$. Hence, the results of this section apply for the energy functional associated with KS-DFT. Theorem 4 establishes for $S \leq 3$ the existence of a self-consistent solution to the eigenvalue problem (Eqn. (39)), which determines the ground-state properties of a materials system.

3.3 Convergence of the finite-element approximation

We now prove the convergence of the finite element approximation. We do so in two steps, first establishing the Γ-convergence of the restricted functional (Theorem 6) and then equi-coercivity (Lemma 7). The main result is Theorem 8. By $\mathcal{P}_k$ we denote the ring of polynomials of non-negative degree less than or equal to k for some fixed $k \geq 1$. Let T_h be a family of triangulations of Ω of decreasing mesh size $h > 0$, and let X_h be the corresponding sequence of subspaces of X consisting of functions whose restriction to every cell in T_h is a polynomial,

$$X_h = \left\{ \tilde{\Psi} \in (H_0^1(\Omega))^N \;\middle|\; \langle \tilde{\psi}_i, \tilde{\psi}_j \rangle_{(L^2(\Omega),L^2(\Omega))} = \delta_{ij},\ i,j = 1,2,\ldots,N,\ \tilde{\psi}_i | T \in \mathcal{P}_k \text{ for } T \in T_h \right\}.$$

In similar vein we introduce a family of subspaces X_{1_h} for the electrostatic problem by

$$X_{1_h} = \left\{ \tilde{\phi} \in H_0^1(\Omega) \;\middle|\; \tilde{\phi} | T \in \mathcal{P}_k \text{ for } T \in T_h \right\}.$$

It follows from approximation theory that the sequence of spaces X_h and X_{1_h} become more and more dense in X and $H_0^1(\Omega)$ as h decreases. We define a sequence of discrete energy functionals

$$\mathcal{E}_h(\Psi,\mathbf{R}) = \begin{cases} \frac{1}{2}\|\nabla\Psi\|^2_{L^2(\Omega)} + G(\rho) + J_h(\rho,\mathbf{R}), & \text{if } \Psi \in X_h, \\ +\infty, & \text{otherwise;} \end{cases}$$

where

$$J_h(\rho,\mathbf{R}) = -\min_{\phi\in H_0^1(\Omega)} I_h(\phi,\rho,\mathbf{R}),$$

and

$$I_h(\phi,\rho,\mathbf{R}) = \begin{cases} I(\phi,\rho,\mathbf{R}) & \text{if } \phi \in X_{1_h},\ \Psi \in X_h, \\ +\infty, & \text{otherwise,} \end{cases}$$

where

$$I(\phi,\rho,\mathbf{R}) = \frac{1}{8\pi}\int_\Omega |\nabla\phi(\mathbf{x})|^2 \mathrm{d}\mathbf{x} - \int_\Omega (\rho(\mathbf{x}) + b(\mathbf{x},\mathbf{R}))\phi(\mathbf{x},\mathbf{R})\,\mathrm{d}\mathbf{x}. \tag{50}$$

The following remark, see Gavini et al. (2007b), is needed before proceeding to the proof of the $\Gamma-$convergence of the finite-element approximation.

Remark 5 *If $(\psi_h)_h \subset (X_h)$ is a sequence such that $\rho_h \to \rho$ in $L^2(\Omega)$, then*

$$\lim_{h\to 0} J_h(\rho_h) = J(\rho)$$

Theorem 6 *Let (A1), (A2) hold and let $S < 4$. Then $\mathcal{E}_h \to \mathcal{E}$ (in the Γ-sense) in the weak topology of X.*

Proof. To establish the $\Gamma-$convergence of the sequence of energy functionals we must establish the $\liminf$ inequality and construct a recovery sequence.

We first show the $\liminf$ inequality. Consider a sequence $(\Psi_h)_h$ such that $\Psi_h \rightharpoonup \Psi$ in X as $h \searrow 0$. We only have to discuss the case that there exists a subsequence $(\Psi_{h_k})_k$ with $\Psi_{h_k} \in X_{h_k}$ for every $k \in \mathbb{N}$. Otherwise the $\liminf$ inequality holds trivially,

$$+\infty = \liminf_{k\to\infty} \mathcal{E}_{h_k}(\Psi_{h_k}, \mathbf{R}) \geq \mathcal{E}(\Psi, \mathbf{R}).$$

By (A1), (A2) and since $S < 4$, it follows as in the proof of Lemma 2 that $\rho_{h_k} \to \rho$ in $L^{\max\{2,q\}}(\Omega)$ for $k \to \infty$. As $\mathcal{E}_h(\Psi, \mathbf{R}) \geq \frac{1}{2}\|\nabla\Psi\|^2_{L^2(\Omega)} + G(\rho) + J_h(\rho, \mathbf{R})$, we find

$$\liminf_{k\to\infty} \mathcal{E}_{h_k}(\Psi_{h_k}, \mathbf{R}) \geq \liminf_{k\to\infty} \left\{ \frac{1}{2}\|\nabla\ \Psi_{h_k}\|^2_{L^2(\Omega)} + G(\rho_{h_k}) + J_{h_k}(\rho_{h_k}, \mathbf{R}) \right\}.$$

From the compact embeddings of X into $L^2(\Omega)$ and $L^q(\Omega)$, Remark 5 which establishes the continuity of the discrete electrostatic problem in $L^2(\Omega)$, the continuity of G in $L^q(\Omega)$ from (c), and the lower semi-continuity of $\|\nabla\Psi_h\|^2_{L^2(\Omega)}$ in the weak topology of X from (d), it follows that

$$\liminf_{k\to\infty} \mathcal{E}_{h_k}(\Psi_{h_k}, \mathbf{R}) \geq \mathcal{E}(\Psi, \mathbf{R}).$$

This establishes the $\liminf$ inequality.

The construction of a recovery sequence is trivial from the density of the finite-element approximation spaces in $H^1(\Omega)$: Let Ψ_h be a sequence constructed from the interpolation functions of successive triangulations such that $\Psi_h \to \Psi$ in X. From the continuity of individual terms of the energy functional, including the discrete electrostatic interaction energy from Remark 5, we have $\lim_{h\to 0} \mathcal{E}_h(\Psi_h, \mathbf{R}) = \mathcal{E}(\Psi, \mathbf{R})$. Hence we conclude $\mathcal{E}_h \to \mathcal{E}$ in the weak topology of X. $\square$

Lemma 7 *Let the assumptions (A2), (A3) hold. Then the family $(\mathcal{E}_h)_{h>0}$ is equi-coercive in the weak topology of X.*

Proof. If $\Psi \notin X_h$, then $\mathcal{E}_h(\Psi, \mathbf{R}) = +\infty$. If $\Psi \in X_h$, then $\mathcal{E}_h(\Psi, \mathbf{R}) = \frac{1}{2}\|\nabla\Psi\|^2_{L^2(\Omega)} + G(\rho) + J_h(\rho, \mathbf{R})$. Also, as the finite-element subspaces X_h and X_{1_h} are constructed from

a single triangulation, this allows us to use each component of $\Psi \in X_h$ as a trial function in the electrostatic problem as demonstrated in Lemma 3 and Eqn. (47). Consequently, we arrive at the inequality

$$J_h(\rho) \geq C_0 \|\Psi\|^3_{L^3(\Omega)} - \frac{C_0}{8\pi}\|\nabla\Psi\|^2_{L^2(\Omega)} - C\|\Psi\|^2_{L^2(\Omega)}$$

for arbitrary $C_0 > 0$. Using the growth results for G,

$$\mathcal{E}_h(\Psi) \geq \frac{1}{2}\left(1 - \frac{C_0}{4\pi}\right)\|\nabla\Psi\|^2_{L^2(\Omega)} + C_0\|\Psi\|^3_{L^3(\Omega)} - c_0\|\Psi\|^{2q}_{L^{2q}(\Omega)} - C\|\Psi\|^2_{L^2(\Omega)} - c_1.$$

Choosing $0 < C_0 < 4\pi$ and since $2q < 3$, the expression on the right hand side is a coercive function independent of h in the weak topology of X. Thus it follows that $\mathcal{E}_h$ is equi-coercive in the weak topology of X. □

Theorem 8 *Let the hypotheses (A1)-(A3) hold and let $S < 4$. Then $\lim_{h\to 0} \inf_X \mathcal{E}_h = \min_X \mathcal{E}$.*

Proof. This result follows from Theorem 6, Lemma 7 and Dal Maso (1993, Theorem 7.8). □

Remark 9 *Theorem 8 establishes rigorously the convergence of the ground state energy of a system computed with a finite-element approximation. Additionally, if the ground-state is not degenerate, the convergence of the ground-state electron density in $H^1_0(\Omega)$ follows.*

3.4 Convergence of the finite-element approximation with numerical quadratures

An efficient implementation of the integrals in the functional requires the further approximation of using numerical quadratures. In this section, we prove the convergence of the finite-element approximation with numerical quadratures. We do so by combining ideas introduced in the previous section with well known estimates of quadrature errors (Ciarlet (2002)).

If $I = \int_\Omega f(\mathbf{x})\,\mathrm{d}\mathbf{x}$ and if $\tilde{I}$ denotes the n-th order quadrature of I, the error associated with the numerical quadrature is given by

$$|\tilde{I} - I| \leq C_\Omega^{n+1} \int_\Omega |D^{n+1} f(\mathbf{x})|\,\mathrm{d}\mathbf{x},$$

where C_Ω is a constant related to the measure of the size of the domain. From now on, we denote the order of the quadrature rule by n, the degree of the polynomial used in the finite-element interpolation by k, and the maximum size of an element in the mesh by h_0. Apparently, $h_0 \to 0$ as $h \to 0$. We define the energy functional where all integrations are performed with numerical quadrature rules (with $Q\{\mathcal{E}\} \equiv \tilde{\mathcal{E}}$ being the quadrature of $\mathcal{E}$) as

$$\tilde{\mathcal{E}}_h(\Psi, \mathbf{R}) = \begin{cases} Q\{\frac{1}{2}\|\nabla\Psi\|^2_{L^2(\Omega)}\} + \tilde{G}(\rho) + \tilde{J}_h(\rho, \mathbf{R}), & \text{if } \Psi \in X_h, \\ +\infty, & \text{otherwise.} \end{cases}$$

Here

$$\tilde{J}_h(\rho, \mathbf{R}) = -\min_{\phi \in H^1_0(\Omega)} \tilde{I}_h(\phi, \rho, \mathbf{R}),$$

and

$$\tilde{I}_h(\phi, \rho, \mathbf{R}) = \begin{cases} \tilde{I}(\phi, \rho, \mathbf{R}) = Q\{I(\phi, \rho, \mathbf{R})\}, & \text{if } \phi \in X_{1_h},\ \Psi \in X_h, \\ +\infty, & \text{otherwise,} \end{cases}$$

The error introduced by the numerical quadrature for the energy functional is given by

$$\begin{aligned} |\tilde{\mathcal{E}}_h(\Psi, \mathbf{R}) - \mathcal{E}_h(\Psi, \mathbf{R})| \leq C h_0^{n+1} \sum_i \int_{e_i} \left| D^{n+1} \Big[\sum_{j=1}^N |\nabla\psi_j|^2 + g(\rho) \Big] \right| \mathrm{d}\mathbf{x} \\ + |\tilde{J}_h(\rho, \mathbf{R}) - J_h(\rho, \mathbf{R})|, \end{aligned}$$

where e_i denotes the i-th element in the finite-element mesh. For $\Psi \in X_h$, $|\nabla\psi_j(\mathbf{x})|$ is a polynomial function of degree $2(k-1)$ for $j = 1, 2, \ldots, N$. Thus, if $n - 2(k-1) \geq 0$, then $D^{n+1}[\sum_{j=1}^N |\nabla\psi_j|^2] = 0$. Hence

$$|\tilde{\mathcal{E}}_h(\Psi,\mathbf{R})-\mathcal{E}_h(\Psi,\mathbf{R})| \leq Ch_0 \sum_i \int_{e_i} \sum_{j=1}^{N} |2g'(\rho)\psi_j(\mathbf{x})\nabla\psi_j(\mathbf{x})|\,\mathrm{d}\mathbf{x} + |\tilde{J}_h(\rho,\mathbf{R})-J_h(\rho,\mathbf{R})|$$
$$\leq Ch_0 \|4(g'(\rho))^2\rho\|^{1/2}_{L^1(\Omega)} \|\nabla\Psi\|_{L^2(\Omega)} + |\tilde{J}_h(\rho,\mathbf{R})-J_h(\rho,\mathbf{R})|. \quad (51)$$

The expression on the right hand side of Eqn. (51) is obtained by using the inverse inequality (Ciarlet (2002)).

We note the following result which has been proved in the previous work (Gavini et al. (2007b)).

Remark 10 *If* $(\Psi_h)_h \subset (X_h)$ *is a sequence such that* $\Psi_h \rightharpoonup \Psi$ *in* X *for* $h \searrow 0$*, if* $n-2k+3>0$*, and* $S<4$*, then* $\lim_{h\to 0} \inf_{H^1_0(\Omega)} \tilde{I}_h(\cdot,\rho_h,\mathbf{R}) = \min_{H^1_0(\Omega)} I(\cdot,\rho,\mathbf{R})$*, i.e.* $\lim_{h\to 0} \tilde{J}_h(\rho_h,\mathbf{R}) = J(\rho,\mathbf{R})$.

We denote by hypothesis (H) the following 3 conditions:

(i) If $(\psi_h)_h \subset (X_h)$ with $\Psi_h \rightharpoonup \Psi$ in X, then $\|(g'(\rho_h))^2\rho_h\|^{1/2}_{L^1(\Omega)}$ is bounded independently of h.

(ii) $S<4$.

(iii) $n-2k+3>0$.

Remark 11 *If hypothesis (H) holds, then* $\lim_{h\to 0}\{\tilde{\mathcal{E}}_h(\Psi_h,\mathbf{R}) - \mathcal{E}_h(\Psi_h,\mathbf{R})\} = 0$.

This follows from Eqn. (51), Remark 5 and Remark 10.

Using these results we proceed to show the convergence of the finite-element approximation with numerical quadratures.

Theorem 12 *Let (A1), (A2) and (H) hold. Then* $\tilde{\mathcal{E}}_h \to \mathcal{E}$ *(in the* $\Gamma-$*sense) in the weak topology of* X.

Proof. Let $(\Psi_h)_h$ be a sequence such that $\Psi_h \rightharpoonup \Psi$. Without loss of generality we may assume the existence of a subsequence $(\Psi_{h_k})_k \subset (\Psi_h)_h$ with $\Psi_{h_k} \in X_{h_k}$ for every k as otherwise it trivially holds

$$+\infty = \liminf_{k\to\infty} \tilde{\mathcal{E}}_{h_k}(\Psi_{h_k}, \mathbf{R}) \geq \mathcal{E}(\Psi, \mathbf{R}).$$

We observe

$$\liminf_{k\to\infty} \tilde{\mathcal{E}}_{h_k}(\Psi_{h_k}, \mathbf{R}) \geq \liminf_{k\to\infty} \mathcal{E}_{h_k}(\Psi_{h_k}, \mathbf{R}) + \liminf_{k\to\infty} (\tilde{\mathcal{E}}_{h_k} - \mathcal{E}_{h_k})(\Psi_{h_k}, \mathbf{R}).$$

It follows from Remark 10 that $\lim_{k\to\infty}(\tilde{\mathcal{E}}_{h_k} - \mathcal{E}_{h_k})(\Psi_{h_k}, \mathbf{R}) = 0$. Consequently,

$$\liminf_{k\to\infty} \tilde{\mathcal{E}}_{h_k}(\Psi_{h_k}, \mathbf{R}) \geq \liminf_{k\to\infty} \mathcal{E}_{h_k}(\Psi_{h_k}, \mathbf{R}) \geq \mathcal{E}(\Psi, \mathbf{R}).$$

This establishes the $\liminf$ inequality.

The construction of a recovery sequence is trivial from the density of the finite-element approximation spaces in $H^1(\Omega)$. Let $(\Psi_h)_h$ be a sequence constructed from the interpolation functions of successive triangulations such that $\Psi_h \to \Psi$ in X. From Eqn. (51) we have

$$\lim_{h\to 0} \tilde{\mathcal{E}}_h(\Psi_h, \mathbf{R}) = \lim_{h\to 0} \mathcal{E}_h(\Psi_h, \mathbf{R}) = \mathcal{E}(\Psi, \mathbf{R}).$$

Hence, we conclude $\tilde{\mathcal{E}}_h \to \mathcal{E}$ in the weak topology of X. $\square$

Lemma 13 *If (A3) and (H) hold, then the energy functional $\tilde{\mathcal{E}}_h$ obtained by numerical quadrature is equi-coercive in the weak topology of X.*

Proof. We observe from Eqn. (46) that if $\Psi \in X_h$,

$$\mathcal{E}_h(\Psi, \mathbf{R}) \geq \frac{1}{2}\left(1 - \frac{C_0}{4\pi}\right)\|\nabla\Psi\|^2_{L^2(\Omega)} + C_0\|\Psi\|^3_{L^3(\Omega)} - c_0\|\Psi\|^{2q}_{L^{2q}(\Omega)} - C\|\Psi\|^2_{L^2(\Omega)} - c_1.$$

Since $2q < 3$, there exist positive constants C_1, C_2 and C_3 such that

$$E_h(\Psi, \mathbf{R}) \geq C_1\|\nabla\Psi\|^2_{L^2(\Omega)} + C_2\|\Psi\|^2_{L^2(\Omega)} - C_3.$$

This implies

$$\tilde{\mathcal{E}}_h(\Psi,\mathbf{R}) \geq C_1\|\nabla\Psi\|^2_{L^2(\Omega)} + C_2\|\Psi\|^2_{L^2(\Omega)} - C_3 - Ch_0\|\Psi\|_{L^2(\Omega)}\|\nabla\Psi\|_{L^2(\Omega)}.$$

So there exists a bound $\overline{h} > 0$ such that for all $h < \overline{h}_0$

$$\mathcal{E}_h(\Psi,\mathbf{R}) \geq K_0\|\nabla\Psi\|^2_{L^2(\Omega)} + K_1\|\Psi\|^3_{L^3(\Omega)} - K_2,$$

where K_0, K_1, and K_2 are positive constants independent of h. From this inequality it follows that $\tilde{\mathcal{E}}_h$ is equi-coercive in the weak topology of X. □

Theorem 14 *Let (A1)-(A3) and (H) hold. Then* $\lim_{h\to 0}\inf_X \tilde{\mathcal{E}}_h = \min_X \mathcal{E}$.

Proof. This result follows from Theorem 12, Lemma 13, and Dal Maso (1993, Theorem 7.8). □

For the LDA approximation of exchange correlation functionals hypothesis (A1)-(A3) hold with $q = 4/3$. Also if $S \leq 3$, it is easy to check that (H)-(i) holds. Choosing appropriate quadrature rules which satisfy $n - 2k + 3 > 0$, the convergence of the self-consistent eigenvalue problem of KS-DFT using a finite-element approximation with numerical quadratures is established.

3.5 Pseudopotential Approximation

The tightly bound core electrons are chemically inactive and hence have a negligible contribution towards determining the physical properties of the system like binding energy and bond length. Further, the core states are localized in the vicinity of the nucleus leading to oscillations of the valence wavefunctions in this region because of the orthogonality requirement. No matter which basis set is used, large number of basis functions are needed to capture these oscillations. Therefore it is convenient to use the pseudopotential

approximation (Pickett (1989)) in which the all electron potential $V_{\text{ext}}(\mathbf{x},\mathbf{R})$ in Eqn. (33) is replaced with an effective potential $V_{\text{ext}}^{\text{PS}}(\mathbf{x},\mathbf{R})$ (or equivalently the energy $E_{\text{ext}}(\rho,\mathbf{R})$ in Eqn. (27) with an effective energy $E_{\text{ext}}^{\text{PS}}(\rho,\mathbf{R})$) and the core (non valence) electrons are eliminated. The idea is that these effective potentials describe the consequences of the core electrons and also represent the valence electrons by nodeless pseudo-wavefunctions. This enables the solution of much larger systems because of the computational advantage gained.

Based on their spatial dependence, pseudopotentials can be broadly classified as local and non-local. The non-local pseudopotentials which include norm conserving (Bachelet et al. (1982); Rappe et al. (1990); Troullier and Martins (1991)) and ultrasoft pseudopotentials (Vanderbilt (1990)) are angular momentum dependent and are designed to accurately reproduce the scattering properties of the all electron potential, thereby ensuring greater accuracy and transferability. They are usually employed in the Kleinman-Bylander form (Kleinman and Bylander (1982)) which is a lot less computationally expensive than the original semi-local form. Below, we prove the existence of minimizers and convergence of the finite-element approximation with numerical quadratures for local as well as non-local pseudopotential approximations.

3.5.1 Local Pseudopotential

A local pseudopotential is an explicit function $V_{\text{ext}}^{\text{PS}}(\mathbf{x},\mathbf{R})$ with $\|V_{\text{ext}}^{\text{PS}}\|_{L^\infty} \leq C$. The local pseudopotential approximation can then be incorporated into our variational formulation by replacing $b(\mathbf{x},\mathbf{R})$ with $b^{\text{PS}}(\mathbf{x},\mathbf{R}) = \nabla^2 V_{\text{ext}}^{\text{PS}}(\mathbf{x},\mathbf{R})$. Consequently, all the results presented in the previous sections are applicable and hence existence of a minimum and convergence of the finite-element approximation with numerical quadratures follow.

3.5.2 Non-local Pseudopotential

A non-local pseudopotential is an operator on the wavefunction ψ. In the Kleinman-Bylander form, it is expressed as

$$V_{\text{ion}}^{J}(\mathbf{x},\mathbf{R}_J)\psi(\mathbf{x}) = V_{\text{loc}}^{J}(\mathbf{x},\mathbf{R}_J)\psi(\mathbf{x}) + \sum_{lm} C_{lm}^{J} u_{lm}^{J}(\mathbf{x},\mathbf{R}_J)\Delta V_l{}^{J}(\mathbf{x},\mathbf{R}_J)\,, \quad J \in \{1,2,\ldots,M\}. \tag{52}$$

where

$$\Delta V_l{}^{J}(\mathbf{x},\mathbf{R}_J) = V_l{}^{J}(\mathbf{x},\mathbf{R}_J) - V_{\text{loc}}^{J}(\mathbf{x},\mathbf{R}_J)\,, \tag{53}$$

$$C_{lm}^{J} = \frac{\int_\Omega u_{lm}^{J}(\mathbf{x},\mathbf{R}_J)\Delta V_l{}^{J}(\mathbf{x},\mathbf{R}_J)\psi(\mathbf{x})\,\mathrm{d}\mathbf{x}}{\int_\Omega u_{lm}^{J}(\mathbf{x},\mathbf{R}_J)\Delta V_l{}^{J}(\mathbf{x},\mathbf{R}_J)u_{lm}^{J}(\mathbf{x},\mathbf{R}_J)\,\mathrm{d}\mathbf{x}}. \tag{54}$$

$V_l{}^{J}(\mathbf{x},\mathbf{R}_J)$ is the ionic pseudopotential component corresponding to the azimuthal quantum number l, $V_{loc}^{J}(\mathbf{x},\mathbf{R}_J)$ is the 'local' ionic potential and $u_{lm}^{J}(\mathbf{x},\mathbf{R}_J)$ represents the pseudo-wavefunction for the valence states of interest, all for a single atom. The superscript and subscript J is for the atom number and m denotes the magnetic quantum number. Therefore

$$V_{\text{ext}}^{PS}(\mathbf{x},\mathbf{R})\psi(\mathbf{x}) = \sum_{J=1}^{M} V_{\text{loc}}^{J}(\mathbf{x},\mathbf{R}_J)\psi(\mathbf{x}) + \sum_{J=1}^{M}\sum_{lm} C_{lm}^{J} u_{lm}^{J}(\mathbf{x},\mathbf{R}_J)\Delta V_l{}^{J}(\mathbf{x},\mathbf{R}_J). \tag{55}$$

Let us redefine $V_{\text{ext}}(\mathbf{x},\mathbf{R}) = \sum_{J=1}^{M} V_{\text{loc}}^{J}(\mathbf{x},\mathbf{R}_J)$, for which we can obtain the corresponding $b(\mathbf{x},\mathbf{R})$. The energy functional for the pseudopotential can therefore be written as

$$\mathcal{E}^{PS}(\Psi,\mathbf{R}) = \mathcal{E}(\Psi,\mathbf{R}) + \mathcal{K}(\Psi,\mathbf{R})\,, \tag{56}$$

where

$$\mathcal{K}(\Psi,\mathbf{R}) = \sum_{i=1}^{N_v}\sum_{J=1}^{M}\sum_{lm}\frac{1}{G_{lm}^{J}}\left|\int_\Omega f(\mathbf{x},\mathbf{R}_J)\psi_i(\mathbf{x})\,\mathrm{d}\mathbf{x}\right|^2\,, \tag{57}$$

$$f(\mathbf{x},\mathbf{R}_J) = u_{lm}^{J}(\mathbf{x},\mathbf{R}_J)\Delta V_l{}^{J}(\mathbf{x},\mathbf{R}_J)\,, \tag{58}$$

$$G_{lm}^{J} = \int_\Omega u_{lm}^{J}(\mathbf{x},\mathbf{R}_J)\Delta V_l{}^{J}(\mathbf{x},\mathbf{R}_J)u_{lm}^{J}(\mathbf{x},\mathbf{R}_J)\,\mathrm{d}\mathbf{x}. \tag{59}$$

N_v is the total number of electrons after the pseudopotential approximation i.e. valence electrons.

We make the assumption that $f \in H_0^1(\Omega)$ and $V_{\text{loc}}^J \in L^\infty(\Omega)$. Since V_{loc}^J is in principle arbitrary, it can be always chosen such that $G_{lm}^J \neq 0$. We also note the following results:

(B1) The functional $\mathcal{K}$ is continuous in $L^2(\Omega)$. This can be easily verified using Hölder's inequality.

(B2) $\mathcal{K} \geq -C_1 \|\Psi\|^2_{L^2(\Omega)}$, where C_1 is a constant dependent on f, G_{lm}^J. This inequality can be easily obtained using Hölder's inequality.

Theorem 15 *Let (A1)-(A3) hold and let $S < 4$. Then $\mathcal{E}^{PS}(\Psi, \mathbf{R})$ has a minimum in X.*

Proof. The lower semi continuity of $\mathcal{E}^{PS}(\Psi, \mathbf{R})$ in the weak topology of X follows from Lemma 2 and (B1). From Lemma 3 and (B2) it is clear that $\mathcal{E}^{PS}(\Psi, \mathbf{R})$ is coercive in the weak topology of X. Therefore from the fundamental theorem of the calculus of variations, see e.g. Dal Maso (1993), $\mathcal{E}^{PS}(\Psi, \mathbf{R})$ has a minimum in X. □

Theorem 16 *Let the hypotheses (A1)-(A3) hold and let $S < 4$. Then $\lim_{h\to 0} \inf_X \mathcal{E}_h^{PS} = \min_X \mathcal{E}^{PS}$.*

Proof. Using the procedure outlined in Theorem 6 along with (B1) gives $\mathcal{E}_h^{PS} \to \mathcal{E}^{PS}$ (in the Γ-sense). The equi-coercivity of $(\mathcal{E}_h^{PS})_{h>0}$ follows from Lemma 7 and (B2). Hence $\lim_{h\to 0} \inf_X \mathcal{E}_h^{PS} = \min_X \mathcal{E}^{PS}$ (Dal Maso (1993, Theorem 7.8)). □

Theorem 17 *Let (A1)-(A3) and (H) hold. Then $\lim_{h\to 0} \inf_X \tilde{\mathcal{E}}_h^{PS} = \min_X \mathcal{E}^{PS}$.*

Proof. Consider $I = \int_\Omega f_1(x) f_2(x)\, \mathrm{d}\mathbf{x} \quad f_1, f_2 \in H_0^1(\Omega)$. The error due to numerical quadrature is

$$|I-\tilde{I}| \leq C_0 h_0^{n+1} \sum_i \int_{e_i} D^{n+1}(f_1 f_2)\,\mathrm{d}\mathbf{x}$$
$$\leq C h_0 \left[\|\nabla f_1\|_{L^2(\Omega)} \|f_2\|_{L^2(\Omega)} + \|f_1\|_{L^2(\Omega)} \|\nabla f_2\|_{L^2(\Omega)} \right]. \tag{60}$$

The last inequality is obtained by using the inverse inequality (Ciarlet (2002)) and Hölder's inequality. Therefore we have $\lim_{h\to 0}\{I-\tilde{I}\} = 0$. Hence it follows from Remark 11 that $\lim_{h\to 0}\{\tilde{\mathcal{E}}_h^{PS}(\Psi_h,\mathbf{R}) - \mathcal{E}_h^{PS}(\Psi_h,\mathbf{R})\} = 0$. Adopting the same procedure as in Theorem 12 we obtain $\tilde{\mathcal{E}}_h^{PS} \to \mathcal{E}^{PS}$ (in the Γ-sense). Using (B2) in Lemma 13 gives the equi-coercivity of $\tilde{\mathcal{E}}_h^{PS}$ in the weak topology of X. From Dal Maso (1993, Theorem 7.8) $\lim_{h\to 0} \inf_X \tilde{\mathcal{E}}_h^{PS} = \min_X \mathcal{E}^{PS}$. □

In this entire section, spin polarization has not been accounted for, as it has no bearing on the analysis/results presented here and only serves to increase the notational complexity. In particular, it is clear from Eqns. (10-17) that even with spin polarization, the required growth condition given by (A2) still holds, ensuring that all the results are applicable.

4 Numerical Implementation

We now turn to the numerical implementation of the variational formulation described in Section 2. The variational problem (Eqn. (25)) is discretized using the finite element method:

$$\psi_{i\sigma}(\mathbf{x}) = \sum_{j=1}^{N_h} \psi_{i\sigma}^j N_j(\mathbf{x}), \tag{61}$$
$$\phi(\mathbf{x}) = \sum_{j=1}^{N_h} \phi^j N_j(\mathbf{x}) \tag{62}$$

to obtain

$$\sum_{j=1}^{N_h}\left[\int_\Omega \frac{1}{2}\nabla N_j(\mathbf{x})\nabla N_k(\mathbf{x}) + V^\sigma_{h,\text{eff}}(\mathbf{x},\mathbf{R})N_j(\mathbf{x})N_k(\mathbf{x})\,\mathrm{d}\mathbf{x}\right]\psi^j_{i\sigma} = \sum_{q=1}^{N_\sigma}\sum_{j=1}^{N_h}\lambda^\sigma_{iq}\psi^j_{q\sigma}\int_\Omega N_j(\mathbf{x})N_k(\mathbf{x})\,\mathrm{d}\mathbf{x}\,, \tag{63}$$

$$\sum_{j=1}^{N_h}\left[\frac{1}{4\pi}\int_\Omega \nabla N_k(\mathbf{x})\nabla N_j(\mathbf{x})\,\mathrm{d}\mathbf{x}\right]\phi^j = \int_\Omega (\rho(\mathbf{x})+b(\mathbf{x},\mathbf{R}))N_k(\mathbf{x})\,\mathrm{d}\mathbf{x}\,, \tag{64}$$

where λ^σ_{iq} are the Lagrange multipliers used to enforce the constraints (Eqn. 26), $V^\sigma_{h,\text{eff}}$ is the discretized V^σ_{eff}, $\sigma \in \{\alpha,\beta\}$, $i \in \{1,2,\ldots,N_\sigma\}$ and $k \in \{1,2,\ldots,N_h\}$. We would like to use Newton's method for solving Eqns. (63) and (64) because quadratic convergence can be achieved in the vicinity of the solution, but its inefficiency in the initial stages of the iteration process when the guess is far away from the solution, limits its usefulness.

As shown in Section 3.1, the variational and eigenvalue problems are equivalent. Hence, Eqn. (63) can be replaced with the generalized eigenvalue problem:

$$\mathbf{A}^\sigma\tilde{\Psi}^\sigma = \epsilon\mathbf{M}\tilde{\Psi}^\sigma, \qquad \sigma \in \{\alpha,\beta\} \tag{65}$$

where

$$\mathbf{A}^\sigma{}_{ij} = \frac{1}{2}\int_\Omega \nabla N_i(\mathbf{x})\nabla N_j(\mathbf{x})\,\mathrm{d}\mathbf{x} + \int_\Omega V^\sigma_{\text{h,eff}}(\mathbf{x},\mathbf{R})N_i(\mathbf{x})N_j(\mathbf{x})\,\mathrm{d}\mathbf{x}\,, \tag{66}$$

$$\mathbf{M}_{ij} = \int_\Omega N_i(\mathbf{x})N_j(\mathbf{x})\,\mathrm{d}\mathbf{x} \tag{67}$$

and $\tilde{\Psi}$ is a vector of the nodal values of the wavefunction. It is clear that Eqn. (65) needs to be solved self-consistently with Eqn. (64). Since large number of finite element basis functions per atom are required (Pask and Sterne (2005)), solving Eqn. (65) is very expensive since linear systems of equations need to be solved repeatedly in the algorithm.

Keeping in mind the above discussion, we propose the following numerical methodology. Since we expect the electron density to decay much more rapidly than the electrostatic potential, the wavefunctions are solved on a significantly smaller domain $\Omega^\Psi \subset \Omega$. We em-

ploy zero Dirichlet boundary conditions for both the wavefunctions and the electrostatic potential on their respective domains. We first construct a coarse Delaunay triangulation $\mathcal{T}_0$ of the domain Ω, with the nodes $\{\mathbf{x}_a^0\}_{a=1}^{N_{h0}}$ positioned at a coarsening rate of $r^{6/5}$ away from the nuclei, considered optimal for capturing the $1/r$ decay with linear interpolation. Such a triangulation has high resolution in Ω^ψ and coarsens away rapidly in $\Omega \setminus \Omega^\psi$, see Fig. 1 for one such triangulation generated for a single atom. It is on this mesh that the atoms reside i.e. all nuclear positions correspond to nodes which trace the path of their respective nuclei.

We solve Eqns. (64) and (65) using the SCF method on $\mathcal{T}_0$, employing the implicitly restarted Lanczos method (Saad (1992)) for solving the eigenvalue problem and the conjugate gradient algorithm for the linear solver. We rewrite Eqn. (65) as

$$(\mathbf{A}^\sigma - \eta\mathbf{M})^{-1}\mathbf{M}\tilde{\Psi}^\sigma = \hat{\epsilon}\tilde{\Psi}^\sigma\,, \tag{68}$$

where η is the shift parameter and $\hat{\epsilon} = \frac{1}{\epsilon-\eta}$. By choosing an appropriate value for η, we 'blow up' part of the eigenvalue spectrum which is of interest, thereby enhancing the rate of convergence of the eigenvalue solver without incurring any additional cost. Also, since $\mathcal{T}_0$ is very coarse, the computational expense involved for this step is minimal. Next, we apply Freudenthal's subdivision algorithm for a 3-simplex (Bey and Aachen (2000)) on $\mathcal{T}_0$ to obtain the triangulation $\mathcal{T}_1$ (Fig. 2), which is an uniform subdivision of $\mathcal{T}_0$ and has nodes at $\{\mathbf{x}_a^1\}_{a=1}^{N_{h1}}$. The solution obtained on $\mathcal{T}_0$ is transferred to $\mathcal{T}_1$ using the shape functions:

$$\theta_a = \theta(\mathbf{x}_a^1) = \sum_{i=1}^{N_{h0}} \theta_i N_i(\mathbf{x}_a^1), \qquad a = 1, \ldots, N_{h1}. \tag{69}$$

This serves as a starting guess for the solution of Eqns. (63) and (64) simultaneously using Newton's method equipped with the Goldstein-Armijo line-search (Dennis and Schnabel (1996)). For the linear solver we use the Generalized minimal residual method (GMRES, Saad and Schultz (1986)) while retaining the option of switching to either the Bi-

Conjugate Gradient Stable method (Bi-CGSTAB, van der Vorst (1992)) or Transpose-Free Quasi-Minimal Residual method (TFQMR, Freund (1993)). The quality of the initial guess enables us to obtain close to quadratic convergence, thereby ensuring that the Newton's algorithm does not require more than 6-7 nonlinear iterations. Consequently, we are able to reach very high accuracy with no significant increase in computational time.

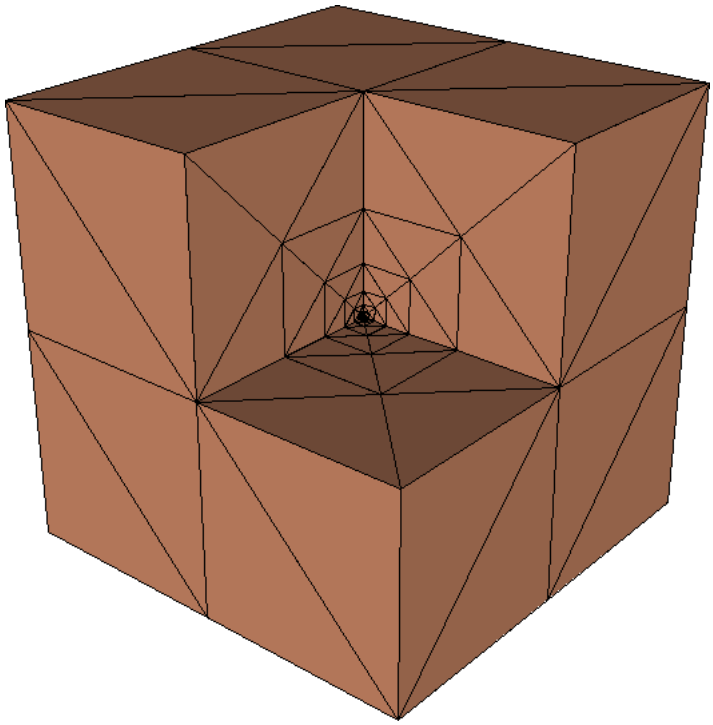

Fig. 1. Mesh of a sliced cubical domain corresponding to the triangulation $\mathcal{T}_0$.

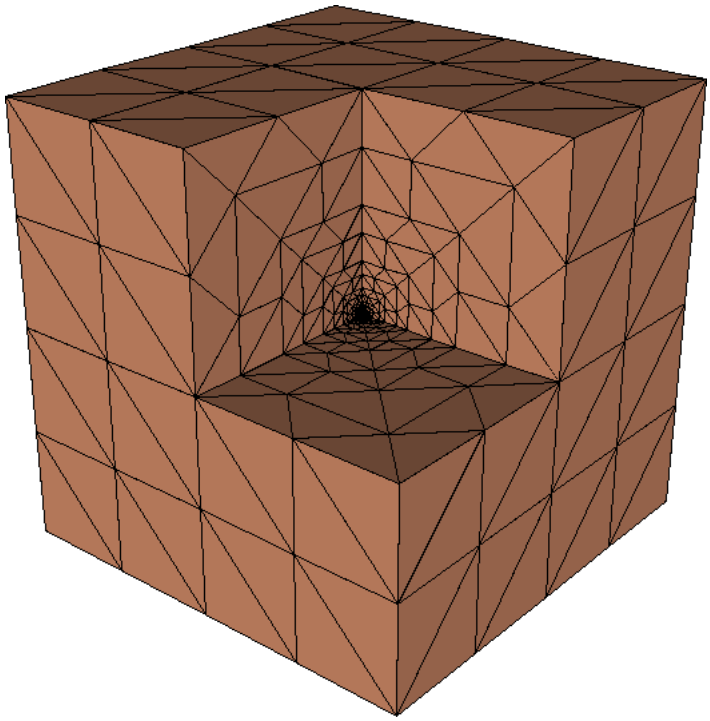

Fig. 2. Mesh of a sliced cubical domain corresponding to the triangulation $\mathcal{T}_1$.

For finding the equilibrium position of the nuclei, we use conjugate gradient with secant line search. The relevant forces are derived in Section 5. We expect that on displacing the nuclei, in the frame of reference attached to each nucleus, there is only a small perturbation in the electrostatic potential and wavefunctions. To take advantage of this fact we employ the following technique. Let $u^i : \quad \mathbb{R}^3 \to \mathbb{R}^3$ denote the deformation of the i^{th} node which has been extended to all nodes of triangulation $\mathcal{T}_0$ by setting it to zero for nodes that do not correspond to nuclei positions, and then linear interpolation is used to encompass Ω:

$$u(\mathbf{x}) = \sum_{i=1}^{N_{h0}} u^i N_i(\mathbf{x}). \tag{70}$$

Subsequently, we deform the mesh $\mathcal{T}_1$ to have nodes at

$$\mathbf{x}_a^u = u(\mathbf{x}_a^1) = \sum_{i=1}^{N_{h0}} u^i N_i(\mathbf{x}_a^1)\,, \qquad a = 1, \ldots, N_{h1}. \tag{71}$$

By doing so, the solution obtained for the previous position of the nuclei serves as a very

good starting guess for Newton's method and again convergence is rapid. The quality of the mesh is kept track off at all times during the computation and if the mesh quality deteriorates below a particular threshold, remeshing is carried out.

Henceforth, the subdivision algorithm is applied repeatedly, whereby a sequence of triangulations $\{\mathcal{T}_n\}$ is generated and the procedure outlined above is used to generate the starting guess and obtain the equilibrium position of the nuclei for every triangulation. This process is continued until we obtain convergence of the solution with respect to mesh size. Since the quality of the starting guess is ever improving, we obtain quadratic convergence at all times. Also, this approach obviates the need for any repeat calculations from scratch which is needed in most numerical schemes. Consider for example, plane wave basis calculations in which convergence has to be verified with respect to the energy cut-off and number of k-points sampled.

Finally, all the computations have been implemented in parallel using the technique of domain decomposition, in which the domain is partitioned into various parts, each of which is handled by a single processor. Since, nearly all the computations are local in nature, we can expect to have good parallel efficiency.

5 Forces

In this section, we derive the forces that determine the equilibrium nuclear configuration. To do so, we assume that for any configuration of the nuclei, the variational problem defined by

$$\inf_{\Psi\in(H_0^1(\Omega))^N} \sup_{\phi\in H_0^1(\Omega)} \mathcal{E}(\Psi,\phi,\mathbf{R}) \tag{72}$$

subject to the constraints $\int \psi^*_{i\sigma}(\mathbf{x})\psi_{j\sigma}(\mathbf{x})\,\mathrm{d}\mathbf{x} = \delta_{ij},\ \sigma\in\{\alpha,\beta\}$, has been solved.

The derivation below closely follows Thoutireddy (2002); Gavini et al. (2007a). Using

Lagrange multipliers to enforce the constraints, we have

$$\begin{aligned}\mathcal{E}_c(\Psi,\phi,\mathbf{R},\Lambda^\alpha,\Lambda^\beta) = \int_\Omega f(\Psi,\nabla\Psi)\,\mathrm{d}\mathbf{x} + \int_\Omega \left(\rho(\mathbf{x})+b(\mathbf{x},\mathbf{R})\right)\phi(\mathbf{x},\mathbf{R})\,\mathrm{d}\mathbf{x} \\ -\frac{1}{8\pi}\int_\Omega |\nabla\phi(\mathbf{x},\mathbf{R})|^2\,\mathrm{d}\mathbf{x} - \sum_{i=1}^{N_\alpha}\sum_{j=1}^{N_\alpha}\lambda_{ij}^\alpha\left(\int_\Omega \psi_{i\alpha}^*(\mathbf{x})\psi_{j\alpha}(\mathbf{x})\,\mathrm{d}\mathbf{x}-\delta_{ij}\right) \\ -\sum_{i=1}^{N_\beta}\sum_{j=1}^{N_\beta}\lambda_{ij}^\beta\left(\int_\Omega \psi_{i\beta}^*(\mathbf{x})\psi_{j\beta}(\mathbf{x})\,\mathrm{d}\mathbf{x}-\delta_{ij}\right). \qquad (73)\end{aligned}$$

In this situation, consider $I_1^h + I_2^h + I_3^h + I_4^h$ where

$$\begin{aligned}I_1^h &= \int_\Omega f(\Psi,\nabla\Psi)\,\mathrm{d}\mathbf{x}\,,\\ I_2^h &= \int_\Omega \left(\rho(\mathbf{x})+b(\mathbf{x},\mathbf{R})\right)\phi(\mathbf{x},\mathbf{R})\,\mathrm{d}\mathbf{x}\,,\\ I_3^h &= -\frac{1}{8\pi}\int_\Omega |\nabla\phi(\mathbf{x},\mathbf{R})|^2\,\mathrm{d}\mathbf{x}\,,\\ I_4^h &= -\sum_{i=1}^{N_\alpha}\sum_{j=1}^{N_\alpha}\lambda_{ij}^\alpha\left(\int_\Omega \psi_{i\alpha}^*(\mathbf{x})\psi_{j\alpha}(\mathbf{x})\,\mathrm{d}\mathbf{x}-\delta_{ij}\right) - \sum_{i=1}^{N_\beta}\sum_{j=1}^{N_\beta}\lambda_{ij}^\beta\left(\int_\Omega \psi_{i\beta}^*(\mathbf{x})\psi_{j\beta}(\mathbf{x})\,\mathrm{d}\mathbf{x}-\delta_{ij}\right).\end{aligned}$$

Note that

$$I_1^h = \int_\Omega f(\Psi,\nabla\Psi)\,\mathrm{d}\mathbf{x} = \sum_{e\in T_h}\int_{\hat\Omega} f(\Psi,\nabla\Psi)\det\left(\frac{\partial\mathbf{x}_M}{\partial\hat{\mathbf{x}}_N}\right)\mathrm{d}\hat{\mathbf{x}}\,,$$

where $\hat\Omega$ is the reference volume in isoparametric formulation and $\frac{\partial\mathbf{x}_M}{\partial\hat{\mathbf{x}}_N}$ is the jacobian of transformation. Taking variations of I_1 we obtain

$$\begin{aligned}\delta I_1^h &= \sum_{e\in\mathcal{T}_0}\int_{\hat\Omega}\left\{-\sum_\sigma\sum_{i=1}^{N_\sigma}\frac{\delta f(\Psi,\nabla\Psi)}{\delta\psi_{i\sigma,J}}\left[\sum_{a=1}^{N_{h0}}\psi_{i\sigma}^a\hat N_{a,A}\frac{\partial\hat{\mathbf{x}}_A}{\partial\mathbf{x}_K}(\sum_{b=1}^{N_{h0}}\delta\mathbf{x}_{bK}^e\hat N_{b,B})\frac{\partial\hat{\mathbf{x}}_B}{\partial\mathbf{x}_J}\right]\right.\\ &\qquad\left.+f(\Psi,\nabla\Psi)(\sum_{b=1}^{N_{h0}}\delta\mathbf{x}_{bK}^e\hat N_{b,B})\frac{\partial\hat{\mathbf{x}}_B}{\partial\mathbf{x}_K}\right\}\det\left(\frac{\partial\mathbf{x}_M}{\partial\hat{\mathbf{x}}_N}\right)\mathrm{d}\hat{\mathbf{x}}\\ &= \sum_{e\in\mathcal{T}_0}\int_{\Omega^e}\left\{-\sum_\sigma\sum_{i=1}^{N_\sigma}\frac{\delta f(\Psi,\nabla\Psi)}{\delta\psi_{i\sigma,J}}\left[\sum_{a=1}^{N_{h0}}\psi_{i\sigma}^a N_{a,K}\right]+f(\Psi,\nabla\Psi)\delta_{KJ}\right\}\left(\sum_{b=1}^{N_{h0}}\delta\mathbf{x}_{bK}^e N_{b,J}\right)\mathrm{d}\Omega\\ &= \sum_{e\in\mathcal{T}_0}\int_{\Omega^e}\left\{-\sum_\sigma\sum_{i=1}^{N_\sigma}\frac{\delta f(\Psi,\nabla\Psi)}{\delta\psi_{i\sigma,J}}\psi_{i\sigma,K}(\mathbf{x})+f(\Psi,\nabla\Psi)\delta_{KJ}\right\}\left(\sum_{b=1}^{N_{h0}}\delta\mathbf{x}_{bK}^e N_{b,J}\right)\mathrm{d}\mathbf{x}\,.\end{aligned}$$

Similarly, note that

$$I_2^h = \int_\Omega \left(\rho(\mathbf{x}) + b(\mathbf{x},\mathbf{R})\right)\phi(\mathbf{x},\mathbf{R})\,\mathrm{d}\mathbf{x} = \sum_{e\in\mathcal{T}_0}\int_{\hat{\Omega}} \left(\rho(\mathbf{x}) + b(\mathbf{x},\mathbf{R})\right)\phi(\mathbf{x},\mathbf{R})\det\left(\frac{\partial \mathbf{x}_M}{\partial \hat{\mathbf{x}}_N}\right)\mathrm{d}\hat{\mathbf{x}}\,.$$

Taking variations, we find

$$\begin{aligned}
\delta I_2^h &= \sum_{e\in\mathcal{T}_0}\int_{\hat{\Omega}} \left(\rho(\mathbf{x}) + b(\mathbf{x},\mathbf{R})\right)\phi(\mathbf{x},\mathbf{R})\left(\sum_{b=1}^{N_{h0}}\delta\mathbf{x}^e_{bK}\hat{N}_{b,B}\right)\frac{\partial\hat{\mathbf{x}}_B}{\partial\mathbf{x}_K}\det\left(\frac{\partial \mathbf{x}_M}{\partial \hat{\mathbf{x}}_N}\right)\mathrm{d}\hat{\mathbf{x}} \\
&\quad + \sum_{e\in\mathcal{T}_0}\int_{\hat{\Omega}} (\delta b)\,\phi(\mathbf{x},\mathbf{R})\det\left(\frac{\partial \mathbf{x}_M}{\partial \hat{\mathbf{x}}_N}\right)\mathrm{d}\hat{\mathbf{x}} \\
&= \sum_{e\in\mathcal{T}_0}\int_{\Omega^e} \left(\rho(\mathbf{x}) + b(\mathbf{x},\mathbf{R})\right)\phi(\mathbf{x},\mathbf{R})\delta_{KJ}\left(\sum_{b=1}^{N_{h0}}\delta\mathbf{x}^e_{bK}N_{b,J}\right)\mathrm{d}\mathbf{x} \\
&\quad + \sum_{e\in\mathcal{T}_0}\int_{\Omega^e} b(\mathbf{x},\mathbf{R})\left(\sum_{a=1}^{N_{h0}}\phi_a N_{a,K}\right)\delta\mathbf{x}^e_{bK}\,\mathrm{d}\mathbf{x}\ .
\end{aligned}$$

Similarly,

$$\begin{aligned}
\delta I_3^h &= -\frac{1}{8\pi}\sum_{e\in\mathcal{T}_0}\int_{\Omega^e}\left\{|\nabla\phi(\mathbf{x},\mathbf{R})|^2\delta_{KJ} - 2\phi_{,J}(\mathbf{x},\mathbf{R})\phi_{,K}(\mathbf{x},\mathbf{R})\right\}\left(\sum_{b=1}^{N_{h0}}\delta\mathbf{x}^e_{bK}N_{b,J}\right)\mathrm{d}\mathbf{x}\,, \\
\delta I_4^h &= -\sum_{i=1}^{N_\alpha}\sum_{j=1}^{N_\alpha}\lambda^\alpha_{ij}\sum_{e\in\mathcal{T}_0}\int_{\Omega^e}\psi^*_{i\alpha}(\mathbf{x})\psi_{j\alpha}(\mathbf{x})\delta_{KJ}\left(\sum_{b=1}^{N_{h0}}\delta\mathbf{x}^e_{bK}N_{b,J}\right)\mathrm{d}\mathbf{x} \\
&\quad -\sum_{i=1}^{N_\beta}\sum_{j=1}^{N_\beta}\lambda^\beta_{ij}\sum_{e\in\mathcal{T}_0}\int_{\Omega^e}\psi^*_{i\beta}(\mathbf{x})\psi_{j\beta}(\mathbf{x})\delta_{KJ}\left(\sum_{b=1}^{N_{h0}}\delta\mathbf{x}^e_{bK}N_{b,J}\right)\mathrm{d}\mathbf{x}.
\end{aligned}$$

Collecting all terms, the force on b^{th} node along the K^{th} direction is given by

$$f^{bK} = \sum_{e\in\mathcal{T}_0}\int_{\Omega^e} Z_b b_b\left(\sum_{a=1}^{N_{h0}}\phi_a N_{a,K}\right)\mathrm{d}\mathbf{x} + \sum_{e\in\mathcal{T}_0}\int_{\Omega^e}\mathrm{E}_{KJ}N_{b,J}\,\mathrm{d}\mathbf{x}\,, \tag{74}$$

where

$$\begin{aligned}
\mathrm{E}_{KJ} &= \left\{f(\Psi,\nabla\Psi) + \left(\rho(\mathbf{x}) + b(\mathbf{x},\mathbf{R})\right)\phi(\mathbf{x},\mathbf{R}) - \frac{1}{8\pi}|\nabla\phi(\mathbf{x},\mathbf{R})|^2\right\}\delta_{KJ} \\
&\quad - \left\{\sum_{i=1}^{N_\alpha}\sum_{j=1}^{N_\alpha}\lambda^\alpha_{ij}\psi^*_{i\alpha}(\mathbf{x})\psi_{j\alpha}(\mathbf{x}) + \sum_{i=1}^{N_\beta}\sum_{j=1}^{N_\beta}\lambda^\beta_{ij}\psi^*_{i\beta}(\mathbf{x})\psi_{j\beta}(\mathbf{x})\right\}\delta_{KJ} \\
&\quad - \sum_{\sigma}\sum_{i=1}^{N_\sigma}\frac{\delta f(\Psi,\nabla\Psi)}{\delta\psi_{i\sigma,J}}\psi_{i\sigma,K}(\mathbf{x}) + \frac{1}{4\pi}\phi_{,J}(\mathbf{x},\mathbf{R})\phi_{,K}(\mathbf{x},\mathbf{R})\,.
\end{aligned} \tag{75}$$

Note that the first term of Eqn. (74) corresponds to the Hellmann-Feynman force on the

nuclei, whereas the second term arises because of the finite element discretization and acts on all the nodes of the triangulation. The latter arises from the need to minimize the energy with respect to the nodal configuration for a fixed number of nodes. Hence it can be used effectively for *a posteriori* mesh adaption. Note that the discretization force is local.

6 Examples and Results

6.1 'All electron' calculations

6.1.1 Atoms

The first set of examples considered are atoms of Helium, Lithium, Carbon, Nitrogen and Oxygen. The triangulation $\mathcal{T}_0$ generated for these atoms, which has roughly 300 nodes, is depicted in Fig 1. The convergence of the ground state energy of the Helium atom on increasing the subdivision number (i.e. number of applications of the subdivision algorithm) is shown in Fig 3. It is clear that there is rapid convergence of the energy on decreasing the mesh size. This is representative of the other examples. Table 1 shows that we reproduce the ground state energies obtained by the highly accurate calculations of Kotochigova et al. (1997). The deviation from experiment reflects the well known deficiencies of LSDA.

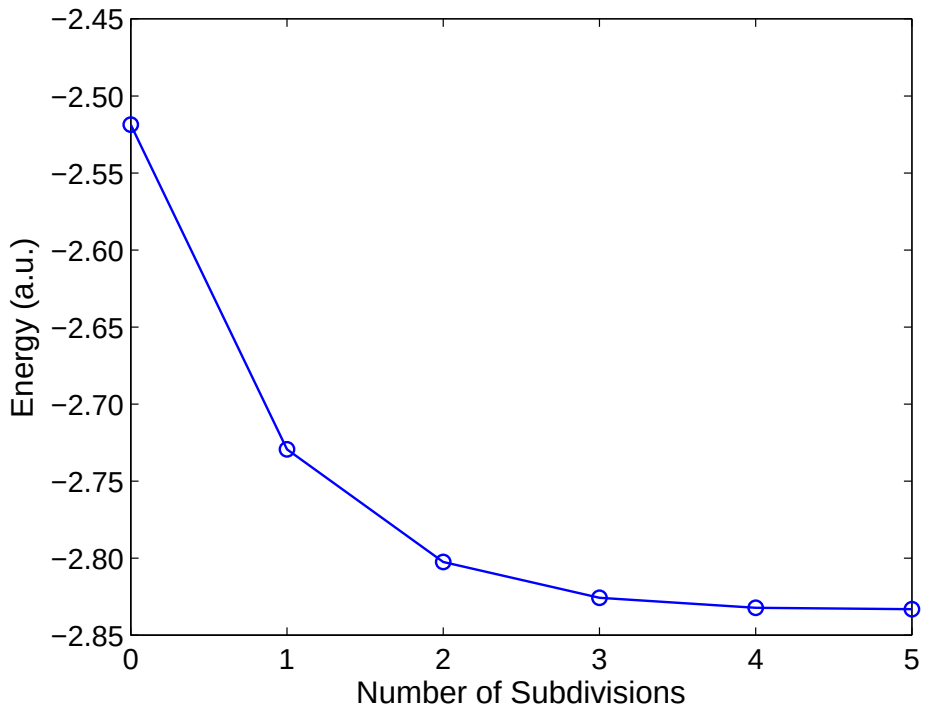

Fig. 3. Energy of the Helium atom as a function of the number of uniform subdivisions of triangulation $\mathcal{T}_0$.

Table 1

Ground state Energies of some atoms (a.u)

Element	KS-DFT-FE (This work)	KS-LSDA (Kotochigova et al. (1997))	KS-LSDA (Perdew and Zunger (1981))	Experiments (Veillard and Clementi (19
He	-2.833	-2.834	-2.833	-2.904
Li	-7.340	-7.343	-7.343	-7.478
C	-37.460	-37.470	-37.466	-37.844
N	-54.125	-54.136	-54.129	-54.587
O	-74.518	-74.527	-74.521	-75.063

6.1.2 Molecules

The next set of examples are nitrogen (N_2) and carbon monoxide (CO) molecules. Tables 2 and 3 show that the binding energy and bond length that we obtain are in very good agreement with values in literature computed using plane waves (Engel et al. (2001)). Again, it is well known that LSDA predicts over binding i.e. higher binding energies and smaller bond lengths compared to experiments. The occupied valence molecular orbitals of CO can be seen in Fig. 4.

Table 2

Binding energy and bond length of N_2

Property	KS-DFT-FE (This work)	KS-LSDA (Engel et al. (2001))	DFT-FE (Gavini et al. (2007b))	Experiments (Huber (1972))
Binding energy (eV)	-11.6	-11.593	-11.9	-9.81
Bond length (a.u.)	2.06	2.068	2.7	2.07

Table 3

Binding energy and bond length of CO

Property	KS-DFT-FE (This work)	KS-LSDA (Engel et al. (2001))	DFT-FE (Gavini et al. (2007b))	Experiments (Huber (1972))
Binding energy (eV)	-13.03	-12.967	-12.6	-11.2
Bond length (a.u.)	2.08	2.128	2.75	2.13

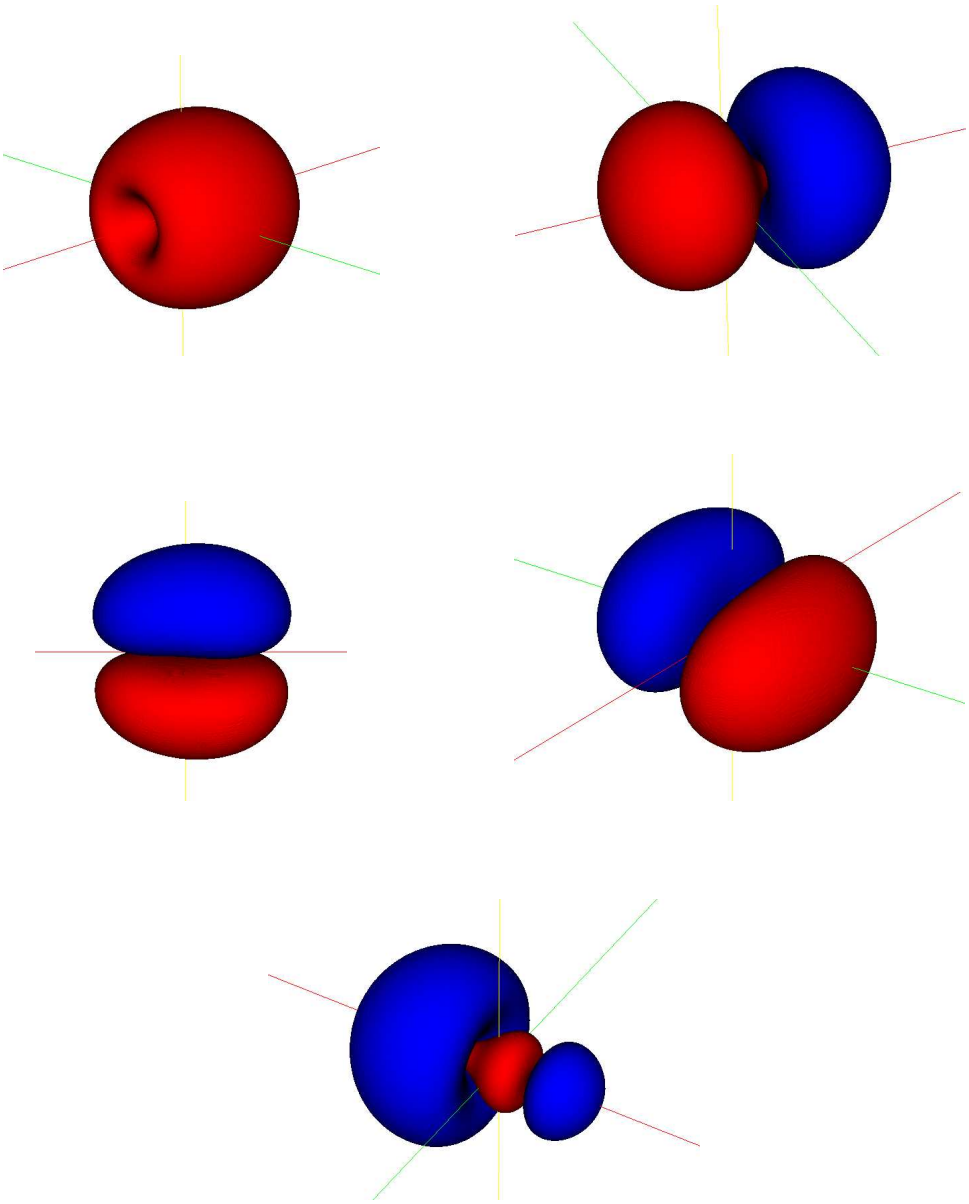

Fig. 4. Occupied valence molecular orbitals of CO.

6.2 Pseudopotential Approximation (Local)

In this section we present the results obtained using the smooth local 'Evanescent Core' pseudopotential (Fiolhais et al. (1995)). This pseudopotential has the form

$$V_{\text{ion}}^{I}(\mathbf{x},\mathbf{R}_I) = -\frac{Z}{R_c}\left\{\frac{1}{y}(1-(1+\beta y)e^{-\alpha y}) - Ae^{-y}\right\} \tag{76}$$

where Z is the number of valence electrons and $y = |\mathbf{x}-\mathbf{R}_I|/R_c$. The core decay length R_c and $\alpha \geq 0$ are element dependent constants whose values can be obtained from Fiolhais et al. (1995). The following relations are used to evaluate β and A

$$\beta = \frac{\alpha^3 - 2\alpha}{4(\alpha^2-1)}, \qquad A = \frac{1}{2}\alpha^2 - \alpha\beta. \tag{77}$$

The pseudopotential approximation is first used to calculate the pseudo-atom energy of Lithium, Sodium and Magnesium. From Table 4, it is clear that we are able to replicate the results obtained by Nogueira et al. (1996). These pseudo-atom energies are further utilized to evaluate the binding energy and bond length of their respective dimers. As is evident from Table 5, the results obtained are in good agreement with previous calculations (Nogueira et al. (1996)).

Table 4

Pseudo-atom energy (eV) using the 'Evanescent Core' pseudopotential

Metal	KS-DFT-FE (This work)	Nogueira et al. (1996)
Li	-5.97	-5.97
Na	-5.21	-5.21
Mg	-23.05	-23.06

Table 5

Binding energy and bond length for some metal dimers using 'Evanescent Core' pseudopotential

Dimer	Property	KS-DFT-FE (This work)	Nogueira et al. (1996)
Li_2	Binding energy (eV)	-0.49	-0.52
	Bond length (a.u)	4.86	4.92
Na_2	Binding energy (eV)	-0.35	-0.46
	Bond length (a.u)	5.72	5.77
Mg_2	Binding energy (eV)	-0.06	-0.04
	Bond length (a.u)	7.12	7.18

Next, we study the properties of some sodium clusters, in particular $1 \times 1 \times 1$, $2 \times 2 \times 2$ and $3 \times 3 \times 3$ Body Centered Cubic (BCC) unit cells. A representative triangulation $\mathcal{T}_0$ used for $2 \times 2 \times 2$ BCC unit cells and its close-up view is shown in Figs. 5 and 6 respectively. We calculate the binding energy per atom and lattice constant for these clusters by computing the energy for various lattice distances and subsequently fitting the data to a cubic polynomial to obtain the point of minimum. The results so obtained are presented in Table 6. Also, the contours of electron density on the mid-plane and quarter-plane of $2 \times 2 \times 2$ BCC unit cells are shown in Figs. 7 and 8 respectively.

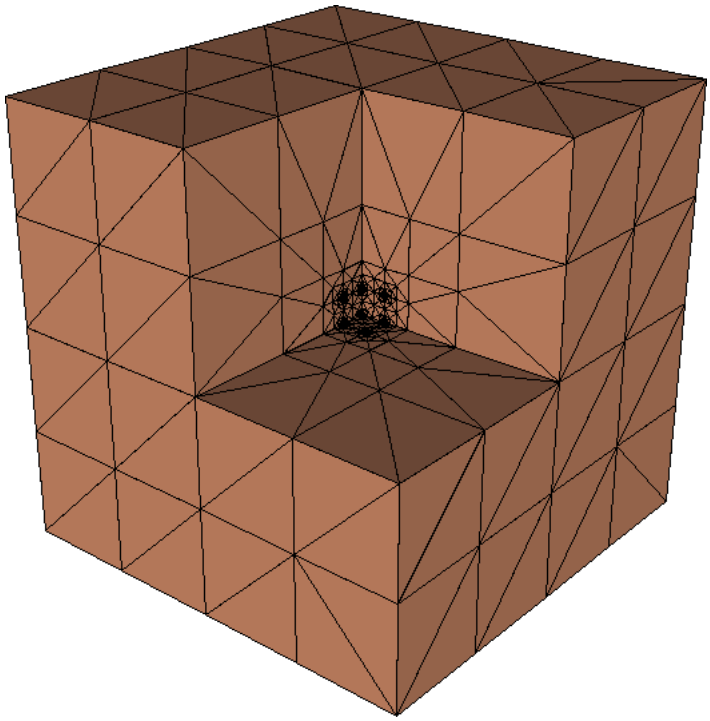

Fig. 5. The triangulation $\mathcal{T}_0$ used for $2 \times 2 \times 2$ BCC unit cells.

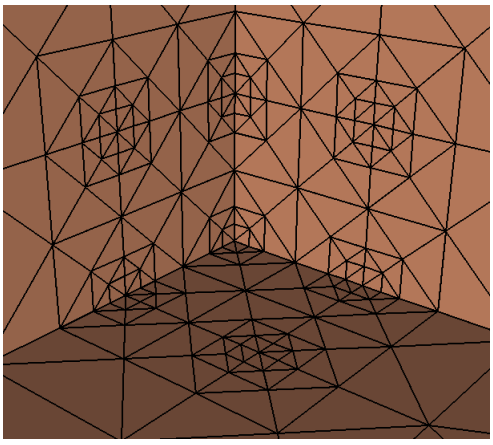

Fig. 6. Close up of the triangulation $\mathcal{T}_0$ used for $2 \times 2 \times 2$ BCC unit cells.

Table 6

Binding energy per atom and lattice constant of Na BCC unit cells

Property	1×1×1	2×2×2	3×3×3
Binding energy/atom (eV)	-0.54	-0.70	-0.81
Lattice constant a (a.u.)	7.20	7.55	7.75

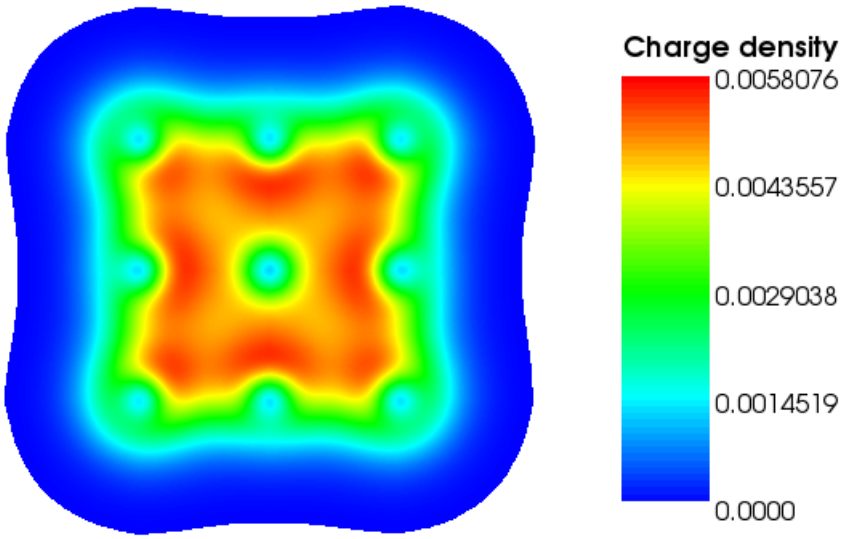

Fig. 7. Contours of electron density on the mid-plane of a sodium cluster with 2×2×2 BCC unit cells.

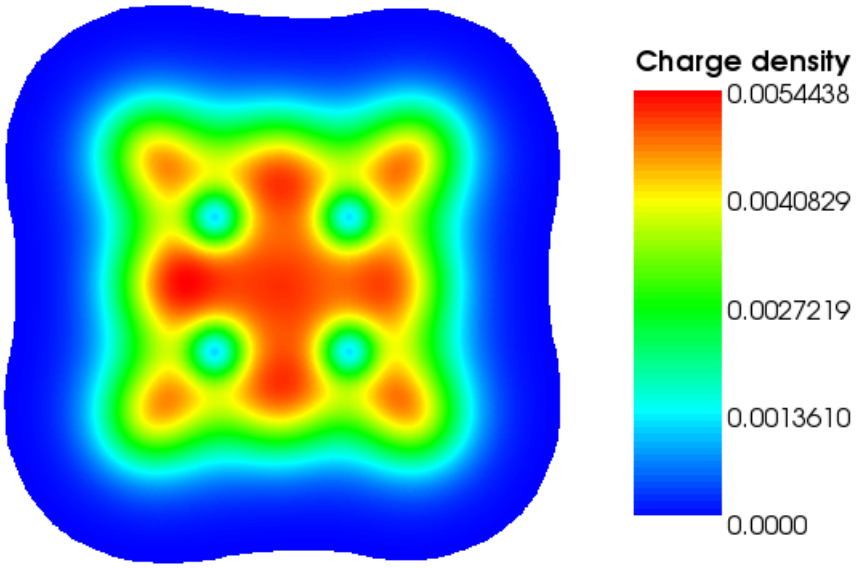

Fig. 8. Contours of electron density on the quarter-plane of a sodium cluster with 2×2×2 BCC unit cells.

6.3 Pseudopotential Approximation (non-local)

Norm conserving pseudopotentials are attractive because of their accuracy, transferability and availability for all elements in the periodic table. Here, we look at the results obtained using the Troullier Martins (TM) pseudopotential (Troullier and Martins (1991)) implemented in the Kleinman-Bylander form.

The radial component of the TM pseudo-wavefunction for an atom located at $\mathbf{R}_I$ is given by

$$w_l(r) = \begin{cases} w_l^{AE}(r)\,, & r \geq r_c\,, \\ r^l \exp[p(r)]\,, & r \leq r_c\,, \end{cases} \tag{78}$$

and the angular momentum dependent pseudopotential component has the form

$$V_l(r) = \begin{cases} V^{AE}(r)\,, & r \geq r_c\,, \\ \epsilon_l + \frac{l+1}{r}\frac{p^{'}(r)}{2} + \frac{p^{''}(r)+(p^{'}(r))^2}{2}\,, & r \leq r_c. \end{cases} \tag{79}$$

The superscript AE stands for 'all electron' calculation, ϵ_l represents the valence eigenvalues, $r = |\mathbf{x} - R_I|$ and r_c is the core radius. The coefficients of the polynomial $p(r) = c_0 + c_2 r^2 + c_4 r^4 + c_6 r^6 + c_8 r^8 + c_{10} r^{10} + c_{12} r^{12}$ are determined by norm conservation, continuity of the pseudo-wavefunction and its first four derivatives and the zero curvature of the pseudopotential at the origin.

In Tables 7, 8 we list the binding energy, bond length of B_2 and C_2 obtained using the TM pseudopotential and compare them with previous such studies (Engel et al. (2001)). The agreement is good, thereby validating the accuracy of our finite element implementation.

Table 7

Binding energy and bond length of B_2

Property	KS-DFT-FE (This work)	Engel et al. (2001)
Binding energy (eV)	-3.70	-3.79
Bond length (a.u.)	3.00	3.02

Table 8

Binding energy and bond length of C_2

Property	KS-DFT-FE (This work)	Engel et al. (2001)
Binding energy (eV)	-6.80	-6.92
Bond length (a.u.)	2.35	2.35

6.4 Performance of the numerical method

This section is directed towards studying various performance related aspects of the numerical method, namely convergence rate with mesh size, scaling of the method with increasing subdivision number and also its parallel scaling. Let us first look at the rate of convergence of the finite element method with decreasing mesh size. It is important to note that since the Kohn-Sham problem is non-linear, standard error estimates (Ciarlet (2002)) do not apply. From Fig. 9, which depicts the normalized error in the energy as a function of the mesh size, we obtain $|\mathcal{E}^h - \mathcal{E}_0| \propto h^{1.9}$, where $\mathcal{E}_0$ is the converged value of the energy obtained by fitting the data to $\mathcal{E} = \mathcal{E}_0 + Ch^n$, where C is a constant.

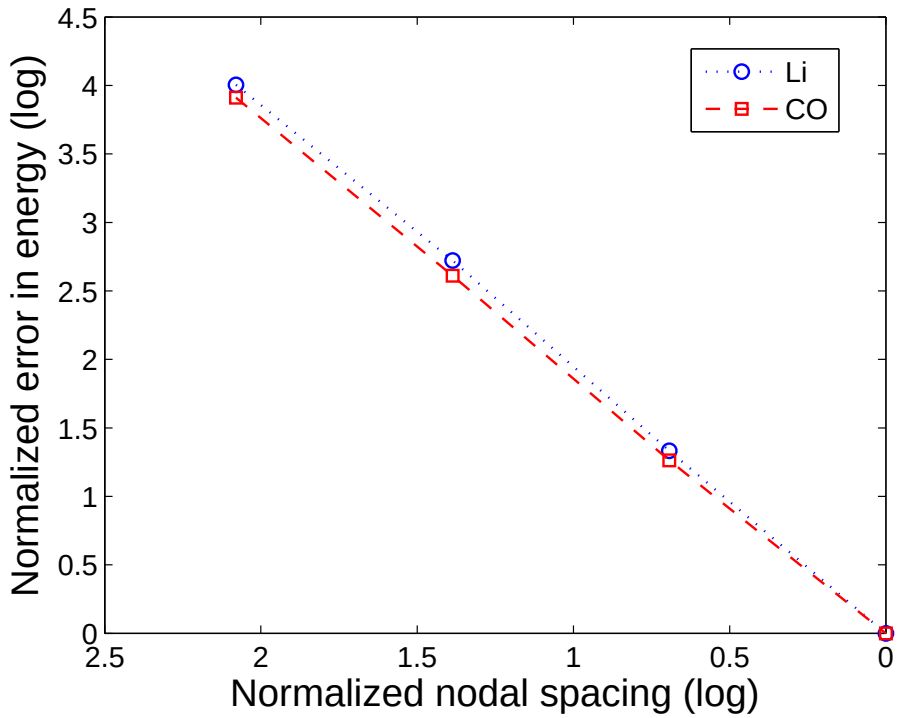

Fig. 9. Convergence rate of the finite-element method.

Next, we look at the computational time as a function of the increasing subdivision level in Fig. 10. The scaling is close to linear, even with an increase in the total number of

nodes by a factor of around ten thousand, confirming the implementation to possess good scaling properties.

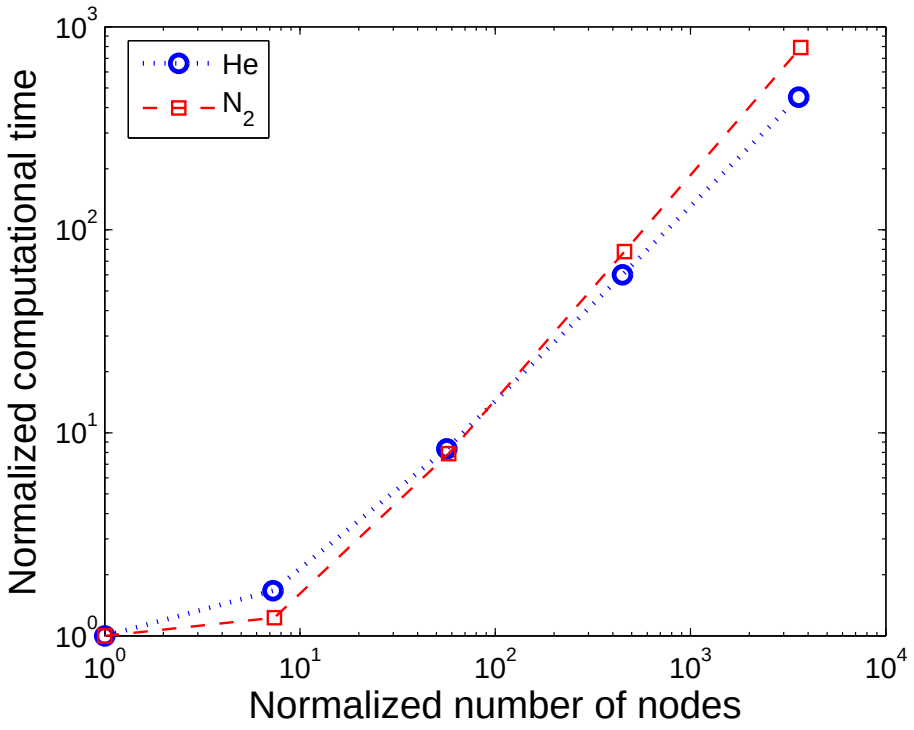

Fig. 10. Scaling of computational time with number of nodes.

Finally, let us check the parallel efficiency of the implementation through its relative speedup with increasing number of processors (Fig. 11). As the number of processors becomes larger, there is a monotonic decrease in the efficiency because of the additional communication required between them. But, even on increasing the number of processors by a factor of 16, there is a relative speedup of 10.25 which translates to an efficiency of about 0.65, thereby ensuring good parallel scaling of the code.

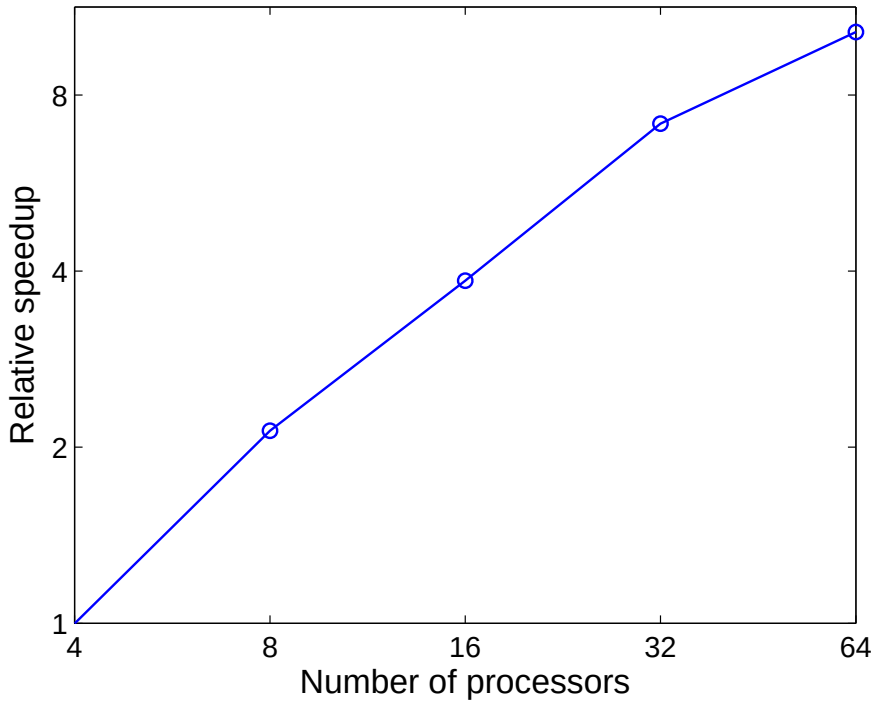

Fig. 11. Relative speedup as a function of the number of processors.

7 Conclusions

We have developed a real space, non-periodic finite-element formulation of KS-DFT in which the minimization of energy has been reformulated as a fully local saddle point problem, thereby resulting in large computational gains. We have shown the well posedness of this formulation for both the 'all electron' problem as well as the pseudopotential approximation, by proving the existence of minimizers and the convergence of its finite-element approximation with numerical quadratures using Γ-convergence. We have also developed a parallel implementation of this formulation capable of performing both 'all electron' and pseudopotential calculations, where the advantageous features of both the SCF method and Newton's method have been utilized to ensure rapid convergence to the solution. The flexibility provided by the unstructured nature of the finite-element mesh

is utilized by optimally coarsening it away from the nuclei and convecting it with the atomic positions, thereby ensuring the efficiency of the calculations without any loss in accuracy. The accuracy of the implementation was tested through a number of examples and the results were found to be in accord with literature. Also, various performance related aspects of the implementation were investigated, including the convergence rate of the finite-element method and its scaling with increasing system size and number of processors. We obtain nearly ideal convergence rate for the finite-element method, close to linear scaling with the number of nodes/elements and a good parallel scaling of the code.

A shortcoming of the present approach and finite elements in general, is the large number of basis functions required to obtain convergence compared to the traditionally used bases like plane waves. This can be reduced by incorporating higher order interpolation functions in our implementation. Another drawback is the difficulty in the generation of efficient meshes for non-trivial geometries of the atoms. These are subjects of current research by the authors. This work is a step towards developing a seamless, multiscale, atomistic-continuum formulation of KS-DFT, with which we hope to study defects in solids. Defects present a unique challenge since quantum mechanical resolution is needed near the core and they also generate long range continuum stresses making finite-elements ideal for their study.

Acknowledgements

References

Bachelet, G. B., Hamann, D. R., Schlüter, M., 1982. Pseudopotentials that work: From H to Pu. Phys. Rev. B 26 (8), 4199–4228.

Bey, J., Aachen, R., 2000. Simplicial grid refinement: on Freudenthal's algorithm and the

optimal number of congruence classes. Numer. Math 85, 1–29.

Bowler, D., Choudhury, R., Gillan, M., Miyazaki, T., 2006. Recent progress with large-scale ab initio calculations: the CONQUEST code. Physica Status Solidi B-Basic Solid State Physics 243 (5), 989–1000.

Castro, A., Appel, H., Oliveira, M., Rozzi, C. A., Andrade, X., Lorenzen, F., Marques, M. A. L., Gross, E. K. U., Rubio, A., 2006. octopus: a tool for the application of time-dependent density functional theory. Physica Status Solidi B-Basic Solid State Physics 243 (11), 2465–2488.

Ceperley, D. M., Alder, B. J., 1980. Ground state of the electron gas by a stochastic method. Phys. Rev. Lett. 45 (7), 566–569.

Chelikowsky, J. R., Troullier, N., Saad, Y., 1994. Finite-difference-pseudopotential method: Electronic structure calculations without a basis. Phys. Rev. Lett. 72 (8), 1240–1243.

Ciarlet, P., 2002. The finite-element method for elliptic problems. SIAM, Philadelphia.

Dal Maso, G., 1993. An introduction to Γ-convergence. Birkhäuser, Boston.

Dennis, J., Schnabel, R., 1996. Numerical Methods for Unconstrained Optimization and Nonlinear Equations. SIAM, Philadelphia.

Engel, E., Höck, A., Schmid, R. N., Dreizler, R. M., Chetty, N., 2001. Role of the core-valence interaction for pseudopotential calculations with exact exchange. Phys. Rev. B 64 (12), 125111.

Finnis, M., 2003. Interatomic forces in condensed matter. Oxford University Press.

Fiolhais, C., Perdew, J. P., Armster, S. Q., MacLaren, J. M., Brajczewska, M., 1995. Dominant density parameters and local pseudopotentials for simple metals. Phys. Rev. B 51 (20), 14001–14011.

Freund, R. W., 1993. A transpose-free quasi-minimal residual algorithm for non-hermitian linear systems. SIAM J. Sci. Comput. 14 (2), 470–482.

Gavini, V., Bhattacharya, K., Ortiz, M., 2007a. Quasi-continuum orbital-free density-functional theory: A route to multi-million atom non-periodic DFT calculation. Journal of the Mechanics and Physics of Solids 55 (4), 697 – 718.

Gavini, V., Knap, J., Bhattacharya, K., Ortiz, M., 2007b. Non-periodic finite-element formulation of orbital-free density functional theory. Journal of the Mechanics and Physics of Solids 55 (4), 669 – 696.

Gilbarg, D., Trudinger, N., 1983. Elliptic differential equations of second order. Springer, New York.

Gonze, X., Beuken, J. M., Caracas, R., Detraux, F., Fuchs, M., Rignanese, G. M., Sindic, L., Verstraete, M., Zerah, G., Jollet, F., Torrent, M., Roy, A., Mikami, M., Ghosez, P., Raty, J. Y., Allan, D. C., 2002. First-principles computation of material properties: the abinit software project. Computational Materials Science 25, 478–492(15).

Hehre, W. J., Stewart, R. F., Pople, J. A., 1969. Self-consistent molecular-orbital methods. I. Use of Gaussian Expansions of Slater-Type Atomic Orbitals. The Journal of Chemical Physics 51 (6), 2657–2664.

Hohenberg, P., Kohn, W., 1964. Inhomogeneous electron gas. Phys. Rev. 136 (3B), B864–B871.

Huber, K., 1972. Constants of diatomic molecules. McGraw-Hill, New York.

Ismail-Beigi, S., Arias, T. A., 2000. New algebraic formulation of density functional calculation. Computer Physics Communications 128 (1-2), 1 – 45.

Kleinman, L., Bylander, D. M., 1982. Efficacious form for model pseudopotentials. Phys. Rev. Lett. 48 (20), 1425–1428.

Kohn, W., 1999. Nobel lecture: Electronic structure of matter—wave functions and density functionals. Rev. Mod. Phys. 71 (5), 1253–1266.

Kohn, W., Sham, L. J., 1965. Self-consistent equations including exchange and correlation effects. Phys. Rev. 140 (4A), A1133–A1138.

Kotochigova, S., Levine, Z. H., Shirley, E. L., Stiles, M. D., Clark, C. W., 1997. Local-density-functional calculations of the energy of atoms. Phys. Rev. A 55 (1), 191–199.

Kresse, G., Furthmüller, J., 1996. Efficient iterative schemes for ab initio total-energy calculations using a plane-wave basis set. Phys. Rev. B 54 (16), 11169–11186.

Langreth, D. C., Mehl, M. J., 1983. Beyond the local-density approximation in calculations of ground-state electronic properties. Phys. Rev. B 28 (4), 1809–1834.

Nogueira, F., Fiolhais, C., He, J., Perdew, J. P., Rubio, A., 1996. Transferability of a local pseudopotential based on solid-state electron density. Journal of Physics: Condensed Matter 8 (3), 287–302.

Parr, R., Yang, W., 1989. Density-functional theory of atoms and molecules. Oxford University Press.

Pask, J. E., Klein, B. M., Fong, C. Y., Sterne, P. A., 1999. Real-space local polynomial basis for solid-state electronic-structure calculations: A finite-element approach. Phys. Rev. B 59 (19), 12352–12358.

Pask, J. E., Sterne, P. A., 2005. Finite element methods in ab initio electronic structure calculations. Modelling and Simulation in Materials Science and Engineering 13 (3), R71–R96.

Payne, M. C., Teter, M. P., Allan, D. C., Arias, T. A., Joannopoulos, J. D., 1992. Iterative minimization techniques for ab initio total-energy calculations: molecular dynamics and conjugate gradients. Rev. Mod. Phys. 64 (4), 1045–1097.

Perdew, J. P., Chevary, J. A., Vosko, S. H., Jackson, K. A., Pederson, M. R., Singh, D. J., Fiolhais, C., 1992. Atoms, molecules, solids, and surfaces: Applications of the generalized gradient approximation for exchange and correlation. Phys. Rev. B 46 (11), 6671–6687.

Perdew, J. P., Wang, Y., 1992. Accurate and simple analytic representation of the electron-gas correlation energy. Phys. Rev. B 45 (23), 13244–13249.

Perdew, J. P., Zunger, A., 1981. Self-interaction correction to density-functional approximations for many-electron systems. Phys. Rev. B 23 (10), 5048–5079.

Pickett, W. E., 1989. Pseudopotential methods in condensed matter applications. Computer Physics reports 9 (3), 115 – 197.

Rappe, A. M., Rabe, K. M., Kaxiras, E., Joannopoulos, J. D., 1990. Optimized pseudopotentials. Phys. Rev. B 41 (2), 1227–1230.

Roothaan, C. C. J., 1951. New developments in molecular orbital theory. Rev. Mod. Phys. 23 (2), 69–89.

Rudin, W., 1991. Functional Analysis. Mc Graw Hill.

Saad, Y., 1992. Numerical Methods for Large Eigenvalue Problems. Manchester University Press.

Saad, Y., Schultz, M. H., 1986. GMRES: A Generalized Minimal Residual Algorithm for Solving Nonsymmetric Linear Systems. SIAM Journal on Scientific and Statistical Computing 7 (3), 856–869.

Segall, M. D., Lindan, P. J. D., Probert, M. J., Pickard, C. J., Hasnip, P. J., Clark, S. J., Payne, M. C., 2002. First-principles simulation: ideas, illustrations and the CASTEP code. Journal of Physics: Condensed Matter 14 (11), 2717–2744.

Skylaris, C.-K., Haynes, P. D., Mostofi, A. A., Payne, M. C., 2005. Introducing [small-caps onetep]: Linear-scaling density functional simulations on parallel computers. The Journal of Chemical Physics 122 (8), 084119.

Soler, J. M., Artacho, E., Gale, J. D., García, A., Junquera, J., Ordejón, P., Sánchez-Portal, D., 2002. The siesta method for ab initio order-n materials simulation. Journal of Physics: Condensed Matter 14 (11), 2745–2779.

Struwe, M., 1990. Variational Methods, Applications to Nonlinear Partial Differential Equations and Hamiltonian Systems. Springer, Berlin.

Thoutireddy, P., 2002. Variational arbitrary lagrangian-eulerian method. Ph.D. thesis, Cal-

ifornia Institute of Technology.

Troullier, N., Martins, J. L., 1991. Efficient pseudopotentials for plane-wave calculations. Phys. Rev. B 43 (3), 1993–2006.

van der Vorst, H. A., 1992. BI-CGSTAB: a fast and smoothly converging variant of BI-CG for the solution of nonsymmetric linear systems. SIAM J. Sci. Stat. Comput. 13 (2), 631–644.

Vanderbilt, D., 1990. Soft self-consistent pseudopotentials in a generalized eigenvalue formalism. Phys. Rev. B 41 (11), 7892–7895.

Veillard, A., Clementi, E., 1968. Correlation energy in atomic systems. v. degeneracy effects for the second-row atoms. The Journal of Chemical Physics 49 (5), 2415–2421.

Wills, J. M., Cooper, B. R., 1987. Synthesis of band and model hamiltonian theory for hybridizing cerium systems. Phys. Rev. B 36 (7), 3809–3823.